UTILIZATION OF STONE WOOL KILN ASH IN SLAG-BASED GEOPOLYMER

TOLGA AYDIN

ÖZYEĞİN UNIVERSITY

JANUARY, 2025

UTILIZATION OF STONE WOOL KILN ASH IN SLAG-BASED GEOPOLYMER

by
Tolga Aydın

Thesis
Submitted in Partial Fulfillment of the
Requirements for the Degree of

Master of Science

in
Civil Engineering

Advisor: Assoc. Prof. Zeynep Başaran Bundur

Graduate School of Science and Engineering
Özyeğin University
İstanbul

January, 2025

UTILIZATION OF STONE WOOL KILN ASH IN SLAG-BASED GEOPOLYMER

Approved by:

Assoc. Prof. Zeynep Başaran Bundur
Advisor
Department of Civil Engineering
Özyeğin University

Assoc. Prof. İlknur Eruçar
Department of Natural Sciences
Özyeğin University

Prof. Nilüfer Özyurt Zihnioğlu
Department of Civil Engineering
Boğaziçi University

Approval Date: December 23, 2024

To my parents,

Filiz & Mesut Aydın

DECLARATION OF ORIGINALITY

I hereby declare that I am the sole author of this thesis and that this is the true copy of my thesis, including the final revisions, approved by my thesis committee. All data and information have been obtained, produced, and presented in accordance with the rules of research ethics and principles of academic honesty. As required by these rules, to the best of my knowledge I have acknowledged ideas, thoughts, and any copyrighted material in accordance with the standard referencing rules. I certify that any part of this thesis has not been submitted for a degree or diploma in another educational institution.

Tolga Aydın

ABSTRACT

Geopolymer production depends on aluminosilicate precursors, yet limited access to industrial by-products necessitates exploring natural alternatives. This study aims to investigate the fresh and hardened properties of geopolymer mortar by utilizing stone wool kiln ash in varying dosages in a one-part ground granulated blast furnace slag (GGBFS)-based, fiber-reinforced geopolymer activated with sodium hydroxide. The fresh and hardened properties were evaluated, including workability, setting time, compressive strength, flexural strength, water absorption, drying shrinkage, and efflorescence and alkali leaching observations. Ultrasonic pulse velocity, a non-destructive test, was also conducted on the produced samples. The microstructural features were also investigated using X-ray diffraction (X-Ray Diffraction (XRD)). The long-term outcomes of this study will provide a roadmap to industry stakeholders, encouraging them to develop new business models to successfully implement raw material transformation and adapt one-part fiber-reinforced geopolymer products for the circular economy. The study will offer insights and recommendations for different geopolymer mix designs and compositions. Finally, the study will contribute to Sustainable Development Goals (SDG) 9, 11, and 13 established by the United Nations.

Keywords: Ground granulated blast furnace slag, Stone wool kiln ash, One-part geopolymer, Mechanical properties, Drying shrinkage

ÖZET

Geopolimer üretimi alüminosilikat öncüllerine bağlıdır, ancak endüstriyel yan ürünlere sınırlı erişim doğal alternatiflerin araştırılmasını gerektirmektedir. Bu çalışmanın amacı, sodyum hidroksit ile aktive edilmiş tek parçalı öğütülmüş granüle yüksek fırın cürufu (GGBFS) bazlı, elyaf takviyeli bir jeopolimerde farklı dozajlarda taş yünü fırın külü kullanarak jeopolimer harcın taze ve sertleşmiş özelliklerini araştırmaktır. Taze ve sertleşmiş özellikler, işlenebilirlik, priz süresi, basınç dayanımı, eğilme dayanımı, su emme, kuruma büzülmesi ve çiçeklenme ve alkali liçi gözlemleri dahil olmak üzere değerlendirilmiştir. Tahribatsız bir test olan ultrasonik darbe hızı da üretilen numuneler üzerinde gerçekleştirilmiştir. Mikroyapısal özellikler de X-ışını kırınımı (XRD) kullanılarak incelenmiştir. Bu çalışmanın uzun vadeli sonuçları, sektör paydaşlarına bir yol haritası sunarak, onları hammadde dönüşümünü başarılı bir şekilde uygulamak için yeni iş modelleri geliştirmeye ve döngüsel ekonomi için tek parça elyaf takviyeli jeopolimer ürünleri uyarlamaya teşvik edecektir. Çalışma, farklı jeopolimer karışım tasarımları ve bileşimleri için içgörü ve öneriler sunacaktır. Son olarak, çalışma Birleşmiş Milletler tarafından belirlenen Sürdürülebilir Kalkınma Hedefleri (SDG) 9, 11 ve 13'e katkıda bulunacaktır.

Anahtar Kelimeler: Öğütülmüş granüle yüksek fırın cürufu, Taş yünü fırın külü, Tek parçalı jeopolimer, Mekanik özellikler, Kuruma rötresi

ACKNOWLEDGEMENTS

I would like to express my deepest gratitude to my advisor, Assoc. Prof. Dr. Zeynep Başaran Bundur, for her invaluable guidance, encouragement, and expertise throughout the development of this thesis and other works. Her insights and unwavering support have been instrumental in shaping this thesis.

This thesis was completed with financial assistance from Türkiye Bilimsel ve Teknolojik Araştırma Kurumu (TÜBİTAK) (Project No: 5220089),(Teknoloji ve Yenilik Destek Programları Başkanlığı (TEYDEB)-1505 University-Industry Collabotation Program (Betek Boya A.Ş).I sincerely appreciate their financial support.

I am also grateful to my thesis committee members, Prof. Dr. Nilüfer Özyurt Zihnioğlu and Assoc. Prof. Dr. İlknur Eruçar, for their invaluable feedback and inspiring suggestions. Their constructive criticism has immensely enriched the quality of research.

This thesis could not have reached completion without the unwavering support of my wonderful colleagues: Ilgın Sandalcı, Shaghayegh Sadeghzadeh Benam, Mahmut Kerem Sarıkaya, Mustafa Can Alp,Sami Berat Taver and Burhan Kara.

I would like to also thank Kaan Aksoy from BETEK Boya for helping and providing materials from BETEK Boya's factory. Also, I would like to also thank Yashar Sardroudi from OzUBEX Sanayi Dönüşüm Merkezi for helping to conduct XRD test.

Lastly, I wish to express my heartfelt gratitude to my family, Filiz Aydın and Mesut Aydın, along with everyone who has supported me in various ways. Their encouragement has fueled my passion and determination, enabling me to reach this significant milestone.

TABLE OF CONTENTS

LIST OF TABLES

LIST OF FIGURES

LIST OF ACRONYMS AND ABBREVIATIONS

GGBFS	Ground Granulated Blast Furnace Slag
UPV	Ultrasonic Pulse Velocity
XRD	X-Ray Diffraction
ASTM	American Society for Testing and Materials
XRF	X-Ray Fluorescence
SEM	Scanning Electron Microscope
TGA	Thermal Gravimetric Analysis
FTIR	Fourier Transform Infrared Spectroscopy
NaOH	Sodium Hydroxide
SF	Silica Fume
MK	Metakaolin
FA	Fly Ash
OPC	Ordinary Portland Cement
C-S-H	Calcium Silicate Hydrates
C-A-H	Calcium Aluminate Hydrates
C-A-S-H	Calcium Aluminosilicate Hydrates
N-A-S-H	Sodium Aluminosilicate Hydrates
OPC	Ordinary Portland Cement
SDG	Sustainable Development Goals
TEYDEB	Teknoloji ve Yenilik Destek Programları Başkanlığı

TÜBİTAK	Türkiye Bilimsel ve Teknolojik Araştırma Kurumu
SCMs	Supplementary Cementitious Materials
KOH	Potassium Hydroxide

1. INTRODUCTION

Ordinary Portland Cement (OPC) is among the most commonly used materials in the modern world right after water owing to its outstanding durability, worldwide accessibility, versatility, and cost-effectiveness [2, 3]. Portland cement production is unsustainable because it consumes large amounts of energy during manufacturing, depletes natural resources and depends on non-renewable energy resources. OPC significantly contributes to environmental pollution, releasing substantial carbon dioxide emissions approximately 7% of global CO_2emissions [4]. As a result, the development and exploration of energy-efficient and environmentally friendly building materials have become key focal points in both the global construction sector and academia on sustainable construction to reduce the environmental footprint of traditional building practices [5, 1]. In recent years, geopolymer has emerged as a promising green, low carbon cementitious material, capturing significant attention and interest from researchers across the globe [6]. It effectively addresses the drawbacks of traditional Portland concrete while offering enhanced mechanical properties, a smaller carbon footprint, and the capability to use industrial waste as raw materials [7, 8]. One of the studies shows that geopolymer concrete can significantly lower greenhouse gas emissions, reducing them by approximately 44–64% compared to traditional Portland cement concrete [9]. As a consequence, geopolymer concrete can significantly diminish CO_2 emissions. The first concept of geopolymers was introduced in the 1970s by French scholar Davidovits [10]. Geopolymer is the result of the geopolymerization process, created through the reaction of aluminosilicate raw materials with alkaline activators [11]. Despite significant research advancements in two-part geopolymers, where the activators are in liquid form, their large-scale practical application remains limited. This is due to their extreme causticity, high corrosiveness, vulnerability to weathering problems,the considerable energy required and the need for stringent safety measures throughout the preparation process [12, 13]. Recently, one-part geopolymers,also known

as just-add-water, can present opportunities beyond the conventional two-part geopolymers since similar to conventional concrete, a solid activator was blended with precursors and mixed with water (so-called "just add water"). Using a one-part geopolymer preserves the advantages of its two-part counterpart, such as durability, thixotropy, and rapid strength development [14]. Additionally, the one-part process reduces the issues and hazards related to handling corrosive liquids. Initially, geopolymers were created through a reaction between metakaolin, a silicon-aluminum-based raw material, and sodium silicate solution as an activator, conducted at room temperature [10]. The raw materials include various industrial wastes such as fly ash , red mud, metakaolin, silica fume, glass powder, and ground granulated blast furnace slag (GGBFS) [15, 16]. Various solid alkaline activators are available for geopolymers, including powdered sodium hydroxide, sodium metasilicate, sodium carbonate, and sodium sulfate [17, 16, 18]. The primary function of alkalis in geopolymerization is to first generate a sufficiently high pH to activate the aluminosilicate raw materials during the geopolymerization process. The geopolymerization mechanism is actually a complex system and three main stages are involved [19, 20] and these stages are dissolution of raw materials in an alkaline solution,reorientation of the dissolved species, and polycondensation to the formation of gel structures, including Calcium Silicate Hydrates (C-S-H),Calcium Aluminate Hydrates (C-A-H),Calcium Aluminosilicate Hydrates (C-A-S-H),and Sodium Aluminosilicate Hydrates (N-A-S-H) [8, 21]. These gels help form a robust geopolymer matrix by creating a rigid, hardened, three-dimensional tetrahedral network structure [22]. Geopolymer concrete outperforms OPC based concrete due to its fast-hardening rate and high strength [23, 24], good thermal stability and high temperature resistance to heat and fire [1, 25], high impermeability and durability [26] and minimal creep effects [27]. Geopolymers have exhibited numerous performance advantages and significant utilization potential, making them a promising new cementitious material. However, several challenges and unresolved issues remain.

These problems can be the instability and volatility of solid waste that affect the properties of the geopolymer, the rapid reaction rate and the high viscosity of geopolymers can lead to poor workability and unmanageable setting times that hinder operational applications, and the absence of consistent and comprehensive standards and specifications [1]. These issues significantly limit the broader application of geopolymers. Up to now, geopolymers have been utilized in plain or fiber-reinforced concrete, as well as in 3D printed structures for structural applications [28, 14]. Additionally, geopolymers was used as one-part foam in insulating components of non-structural elements [29]. They also show promise as coatings for structural concrete repairs [30]. Recently, construction debris has emerged as a promising solution for use as a precursor material. The term ”construction debris” refers to the waste generated during demolition, including materials such as bricks, ceramic wall tiles, and recycled concrete [31, 32]. Additionally, insulation boards made from stone wool products are another form of waste generated from construction debris. A ”zero-waste” approach can only achieve a fully circular production process. The ashes produced from the coke-fired hot blast kiln represent significant waste generated during stone wool production. According to industry stakeholder data, at least 40 tons of ash are produced monthly from a 3000-ton stone wool production. Producers need to valorize the waste stream generated during production to promote sustainable circular production in the stone wool industry. Currently, the principles of the circular economy for stone wool compos- ites are primarily applied when recycled as construction demolition debris [33]. To achieve sustainable circular production for stone wool, it is becoming increasingly important for producers to valorize the waste stream generated during production. Therefore, this thesis aims to provide extensive insight into the valorization of stone wool kiln ash in one part fiber reinforced geopolymer concrete and analyze the impact on matrial’s engineering properties while maintaining its sustainability. These properties include compressive strength, flexural strength, water absorption, flowability, setting time,

drying shrinkage, UPV, XRD , efflorescence, and alkali leaching. The percentage of stone wool kiln ash played a significant role in affecting the mechanical properties, fresh state properties and the microstructural characteristics of one-part geopolymer concrete.

1.1 Goal and Objectives

This study investigates the design of one-part geopolymers by incorporating stone wool kiln ash as part of the precursor material. To the authors' knowledge, no prior research has examined the combined use of stone wool kiln ash and GGBFS as precursors in one-part fiber-reinforced geopolymers activated with sodium hydroxide. The main experimental plan of this study includes evaluating the effect of varying stone wool kiln ash contents on the fresh and hardened properties of one-part fiber-reinforced geopolymer mortars activated with sodium hydroxide (NaOH). To achieve the main goal, the following key scientific objectives were defined:

- Determination of the optimum content of the precursor, alkali activator, water, sand, and fiber.
- Quantifying the fresh state properties such as flowability and setting time of the one-part fiber reinforced geopolymer.
- Quantifying the hardened state properties such as compressive strength, flexural strength, drying shrinkage, water absorption, efflorescence and ultrasonic pulse velocity of the one-part fiber reinforced geopolymer.
- The long-term outcomes of this study will provide a roadmap to industry stakeholders, encouraging them to develop new business models to successfully implement raw material transformation and adapt one-part fiber-reinforced geopolymer products for the circular economy.

- The study will offer insights and recommendations for different geopolymer mix designs and compositions.
- Finally, the study will contribute to Sustainable Development Goals (SDG) 9, 11, and 13 established by the United Nations.

1.2 Outline of the Thesis

This thesis study is established as follows:

- **Chapter 1.** introduces the concept of geopolymer concrete.
- **Chapter 2.** reviews existing literature, assessments of geopolymer concrete by other researchers,and previously tested mixture compositions.
- **Chapter 3.** outlines the materials and methods, providing a comprehensive explanation of the mixing process, mixture formulations, and analysis techniques.
- **Chapter 4.** presents and discusses the results related to the fresh and hardened properties of the fiber-reinforced geopolymer mortar.
- **Chapter 5.** concludes the study by summarizing key findings and their significance.

2. LITERATURE REVIEW

Cement and concrete are two of the most widely used materials globally. Annually, approximately 4.1 billion tons of cement are produced, which translates to about half a ton for every person on Earth. Notably, China accounts for half of this total production [34]. Furthermore, each year, more than 1 cubic meter of concrete per capita is produced, primarily using Portland cement[35]. Due to the globalization and the development of cement technology, modern housing and new city buildings with the usage of cement have accelerated. However, these actions have initiated new environmental problems such ash global climate change, depletion of natural resources, releasing high amounts of CO_2 emissions. As a result, one of the primary environmental challenges in the construction industry today is the demand for eco-friendly building materials that promote sustainable development. Many researchers have suggested various alternatives to OPC by partially replacing it with Supplementary Cementitious Materials (SCMs) to reduce its adverse environmental impact. Common SCMs consist of industrial byproducts like Fly Ash (FA), Ground Granulated Blast Furnace Slag (GGBFS),Silica Fume (SF),and Metakaolin (MK) [21]. The interest in these SCMs was driven by their local availability as natural or waste materials, along with their specific chemical composition that allowed for the substitution of various amounts of clinker without negatively impacting the performance of cementitious materials [4]. A recently introduced approach involving the use of SCMs in the design and development of geopolymer materials has been reported to reduce CO_2 emissions and energy consumption by $\%60–80\%$ compared to OPC [36]. These materials are made by combining solid aluminosilicate precursors with alkaline solutions or activators, forming a rigid 3-D polymer network that performs the same binding function as OPC [37, 22].

2.1 Reaction mechanism of geopolymers

TThe reaction mechanism of geopolymers synthesized from low-calcium aluminosilicate precursors predominantly encompasses three key stages: dissolution, reorientation, and solidification [19]. The reaction mechanism is shown in **Figure 2.1.** Under the action of an alkali activator, the chemical bonds in aluminosilicate minerals break down, releasing silicon-oxygen and aluminum-oxygen tetrahedron monomers. These monomers first combine to form dimers, which then react with other monomers to create trimers and larger multimers. Eventually, these structures rearrange and undergo polycondensation, resulting in the formation of an amorphous sodium aluminosilicate hydrate (N-A-S-H) gel with a three-dimensional network structure. In contrast, geopolymers synthesized from high-calcium aluminosilicate materials (e.g., slag powder, high-calcium fly ash) typically form two types of gels: sodium aluminosilicate hydrate (N-A-S-H) and calcium silicate hydrate (C-S-H). The concentration of the activator is crucial for the formation of gel structures in geopolymers. If the activator dosage is below a critical threshold, a significant portion of the aluminosilicate precursors will remain unreacted, as there is an inadequate reaction medium for geopolymerization [38]. Conversely, excessive use of the alkali activator can weaken the gel network, leading to reduced mechanical properties. This occurs because an overly high activator dosage can over-extract silica or alumina, leaving insufficient material for polymerization, which hinders the overall reaction [22].

2.2 Common aluminosilicate precursors and alkali activators

The most commonly used materials as precursors for geopolymers are fly ash, silica fume, ground granulated blast furnace slag, and metakaolin. Fly ash is a by-product material produced from burning coal and is classified into two categories based on the chemical composition, Class F and Class C. Class F fly ash is composed of at least 70% silicon dioxide (SiO_2), aluminum oxide (Al_2O_3), and iron oxide (Fe_2O_3). In comparison,

Figure 2.1: *Reaction mechanism of geopolymer [1]*

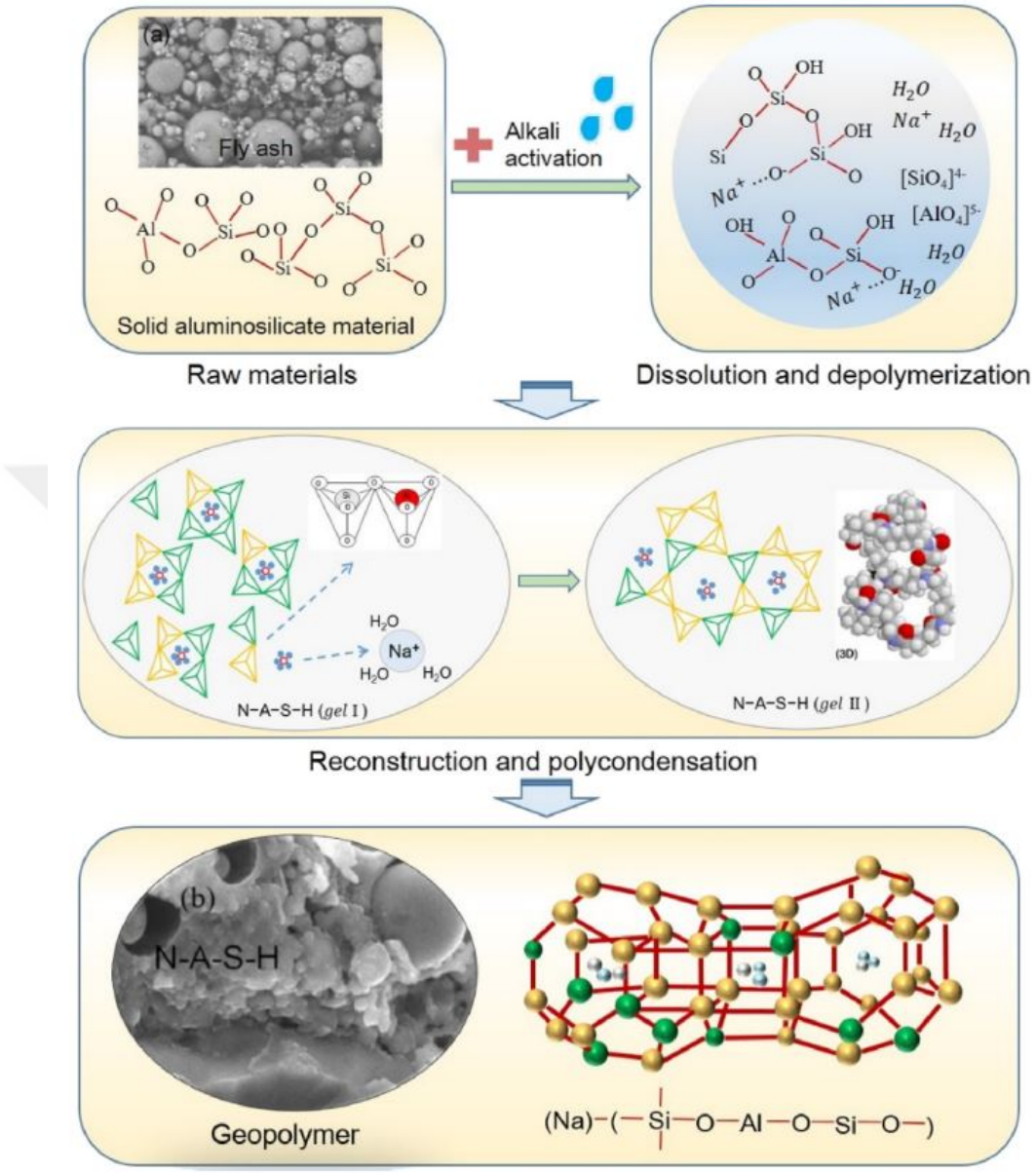

Class C fly ash contains these components in amounts of at least 50% of its chemical composition and contains more than 20% CaO[39].Silica fume is a fine pozzolanic by-product produced during the manufacturing of ferrosilicon or silicon alloys in electric arc furnaces. It is primarily composed of amorphous silica [40]. In the production of geopolymer, ground granulated blast furnace slag (GGBFS) can serve as a primary binder [41].

GGBFS is widely used in one-part geopolymers, with an annual generation rate ranging from 270 to 390 million tons [42].GGBFS, a by-product of iron manufacturing, is produced by collecting the molten material formed when iron is heated to temperatures as high as 1600°C in a blast furnace. The molten product is then rapidly quenched, resulting in GGBFS with a glassy phase [43]. The chemical composition of GGBFS primarily consists of CaO, MgO, $\mathrm{Al_2O_3}$, and $\mathrm{SiO_2}$ [43]. On average, GGBFS contains 90–95% glassy phase, with minor crystalline phases such as gehlenite and akermanite [44]. The particles of GGBfS have an angular and irregular shape [45]. According to numerous studies, slag-based geopolymer mortars and concretes offer superior performance such as rapid initial strength development, attain high compressive strengths, demonstrate excellent durability, and show enhanced resistance to chemicals, as well as better heat resistance when compared to OPC [46, 47]. Metakaolin is produced by heating kaolinite clay to high temperatures between 600 and 900°C, a process known as calcination [48].

For alkaline activators, sodium metasilicate is commonly used as a solid activator in one-part geopolymers [49, 50]; however, it is considered less sustainable due to the high energy required for its activation and production [21]. In addition to sodium metasilicate, other alkali activators, such as Sodium Hydroxide (NaOH) and Potassium Hydroxide (KOH), have also been explored. Among these, NaOH is typically preferred over KOH due to its lower cost, less corrosive nature, and its ability to provide better strength at ambient temperatures [22].

2.3 Geopolymer mix design compositions in literature

Various SCMs compositions with different solid activators have been developed and established for geopolymers. Shoaei et al. [2] explored the potential of using natural zeolite as a component of the precursor in one-part GGBFS-based geopolymer mortars, activated with sodium metasilicate. Their findings revealed that the mechanical strength

shows a decreasing trend with increasing replacement ratios of slag with zeolite. Additionally, a higher zeolite content in the binder composition led to a less dense microstructure. Özen et al. [17] examined the effect of incorporating nano-silica in one-part sodium carbonate-activated slag/r-MgO-based mixes. They concluded that slag-based one-part sodium carbonate-activated mixes demonstrated significantly lower environmental impacts compared to OPC mixes and addition of nano-silica contributed to a denser microstructure and higher gel phase observed in SEM images. Zhang et al. [51] investigated the effect of silica fume on the drying shrinkage behavior of GGBFS-fly ash based geopolymer. Their findings indicate that increasing the content of silica fume effectively reduces the drying shrinkage of the geopolymer paste. This beneficial effect is attributed to the improved microstructure of the geopolymer, as silica fume aids in creating a denser network of calcium silicate hydrate (C-S-H) gel. Murali et al. [52] assesed the effect of silica fume and glass powder in GGBFS-based ultra high-performance geopolymer fibrous concrete. It was concluded that compressive strength gradually increased with the addition of silica fume, reaching its peak at a substitution rate of 10%. Alhamoud et al. [53] studied the engineering properties of slag-based one-part geopolymer concrete and they found that higher ratios of metasilicate led to a reduction in unreacted GGBFS particles, which in turn improved gel formation and increased compressive strength. Ou et al. [54] investigated the effects of fly ash and silica fume contents on the slump, compressive strength, and drying shrinkage behavior of alkali-activated slag concrete. The findings enlightened that the inclusion of fly ash and silica fume both helped to reduce the final drying shrinkage. Yu et al. [55] examined the both macro-mechanical properties and microstructural characteristics of fly ash-based geopolymers activated with various types and amounts of calcium-based activators. The results revealed that the unconfined compressive strength of geopolymer samples increased as the activator dosage was raised. Among activators used at the same dosage, the unconfined compressive strength ranked in

descending order as follows: compound calcium hydroxide, calcium sulfate, and calcium hydroxide. Qiao et al. [56] studied how varying the fly ash-to-metakaolin ratio and the concentration of the activator influenced the mechanical properties and microstructural characteristics of fly ash-metakaolin based geopolymer pastes. The key findings of this study emphasized that the compressive strength of metakaolin-fly ash-based geopolymer pastes showed a gradual decline with an increase in fly ash content. In contrast, higher activator concentrations enhanced compressive strength. Furthermore, as the fly ash content increased, the proportion of the amorphous gel phase diminished, while the intensity of quartz and mullite diffraction peaks became more pronounced. Xiaoshuang et al. [57] inspected the preparation of geopolymer mortar using a ternary mixture of slag, red mud, and fly ash. The results indicated that red mud can be replaced with fly ash due to similar effects in mechanical properties. Moreover,slag improved mechanical properties and accelerates setting time. Higher slag content introduced additional CaO into the matrix, promoting the formation of denser C-S-H gel. This results in enhanced flexural and compressive strength of the geopolymer mortar. Ren et al. [49] assesed the impact of pure $\mathrm{CaCO_3}$ incorporation on sodium metasilicate-activated metakaolin-based geopolymer pastes, focusing on hydration kinetics, mechanical strength, and microstructural evolution. The experimental results displayed that the replacement of 10% $\mathrm{CaCO_3}$ enhanced the overall geopolymerization reaction degree in metakaolin-based geopolymers. However, samples with 50% $\mathrm{CaCO_3}$ exhibited low compressive strengths across the entire curing period. Longhi et al. [58] evaluated the effects of air carbonation,efflorescence formation, and leaching in metakaolin based geopolymers on mechanicals strength and micro/nanostructure.The findings underlying that efflorescence formation causes excessive superficial deterioration in matrix and crystal formation within the pores, generating internal stress and decreasing mechanical properties. Dadsetan et al. [59] studied the impact of glass powder on the rheological, mechanical, and microstructural properties of

metakaolin-based geopolymer pastes. The results showed that the optimal amounts of reactive Si and Al, along with higher sodium concentration, increased the dissolution rate, leading to the formation of more hydrated sodium aluminosilicate gels. Additionally, in geopolymers with a lower SiO_2/Al_2O_3 ratio, many unreacted particles and disconnected reaction products were observed, indicating a less number of siloxo units (-Si-O-). Srinivasa et al. [60] analyzed the impact solid activators on the flowability and compressive strength properties of one-part geopolymer pastes made from fly ash and GGBFS. According to experimental test results, flowability decreases with higher slag content due to its particle morphology and CaO content, while increasing activator content improves flow due to excess sodium silicate hindering raw material dissolution, leading to a less cohesive paste. Tuyan et al. [61] investigated the impact of alkali activator concentration and curing conditions on the flowability, mechanical properties, and microstructure of geopolymer made from waste clay brick powder. The results exhibited that the optimal alkali activator concentration was determined to be 10% Na_2O, and the flow diameter of the mixtures increased with higher Na_2O content. Chaitanya et al. [62] looked into to the effects of substituting rice husk ash for fly ash on the microstructural and strength characteristics of geopolymer concrete.The SEM analysis revealed that the resulting geopolymer concrete is well-compacted, has a dense matrix, and contains few pores.

3. MATERIALS AND METHODS

3.1 Materials

GGBFS obtained from Oyak Çimento, Turkey, was used as the main binder in this study, and stone wool kiln ash, supplied from BETEK Boya, Turkey, was replaced with GGBFS. The particle size distribution curves of the GGBFS and stone wool kiln ash are illustrated in **Figure 3.1.** The GGBFS used in this study had an average diameter (D_{50}) of about 9.35 µm, whereas the average diameter of stone wool kiln ash was 22.8 µm. Furthermore, the GGBFS and stone wool kiln ash have a specific surface area of 1603 and 857.4 m^2/kg, respectively. The X-Ray Fluorescence (XRF) analysis results of GGBFS and stone wool kiln ash are shown in **Table 3.1.** It can be observed that the dominant compounds were CaO,SiO_2,Al_2O_3, and K_2O. NaOH($\%99$ purity) was utilized as an alkali activator for geopolymerization raction. Quartz fine sand (SiO_2 concentration (%w /w) between 90-100%) was used as aggregate, and the gradation curve of the sand is depicted in **Figure 3.2.**. The D_{50} of sand was 0.401 mm. The selection of fine sand is primarily based on two factors: 1) its suitability for plaster mortar and thin board applications, and 2) its compatibility with 3D printing technology.

Table 3.1: *Chemical compositions of slag and stone wool kiln ash*

Chemical composition (% by weight)	**GGBFS**	**Stone wool kiln ash**
SiO_2	27.53	40.30
Al_2O_3	9.55	1.24
Fe_2O_3	0.71	4.91
CaO	52.74	4.39
MgO	4.05	7.43
SO_3	1.58	5.14
Na_2O	0.33	7.14
K_2O	0.84	14.10
TiO_2	1.91	0.15
Loss of ignition (%)	0.26	7.65

Table 3.2: *Physical properties of polypropylene microfiber*

Type	Long monofilament
Density	0,91 g/cm^3
Tensile strength	467-548 MPa
Melting point	160°C
Diameter	32 µm
Length	12 mm
Appearance	Transparent fibres

Figure 3.1: *Particle size distribution of binders, GGBFS: Ground granulated blast furnace slag*

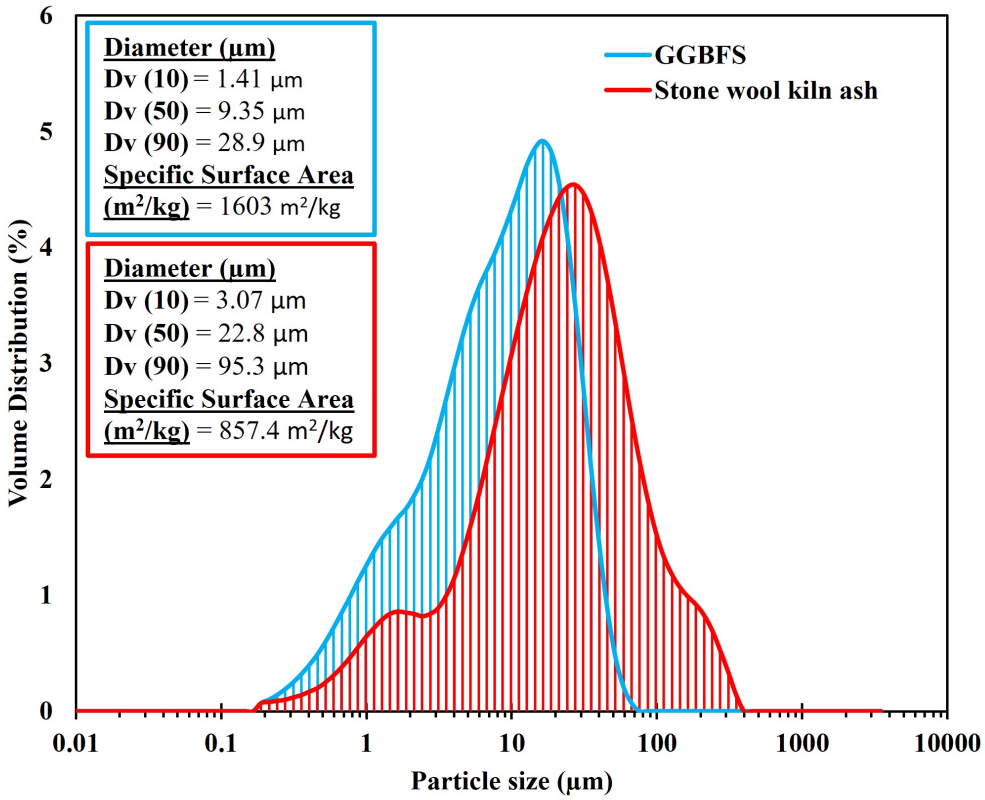

3.2 Mix design and sample preparation

The characteristics of geopolymer pastes and mortars were investigated by varying slag-to-stone wool kiln ash ratios to explore the influence of binder composition. A total of 4 separate mixes shown in **Table 3.3.** were prepared in both paste and mortar. The binder content was kept at 1200 grams in all mixes. The mixes were named based on

Figure 3.2: *Gradation curve of sand*

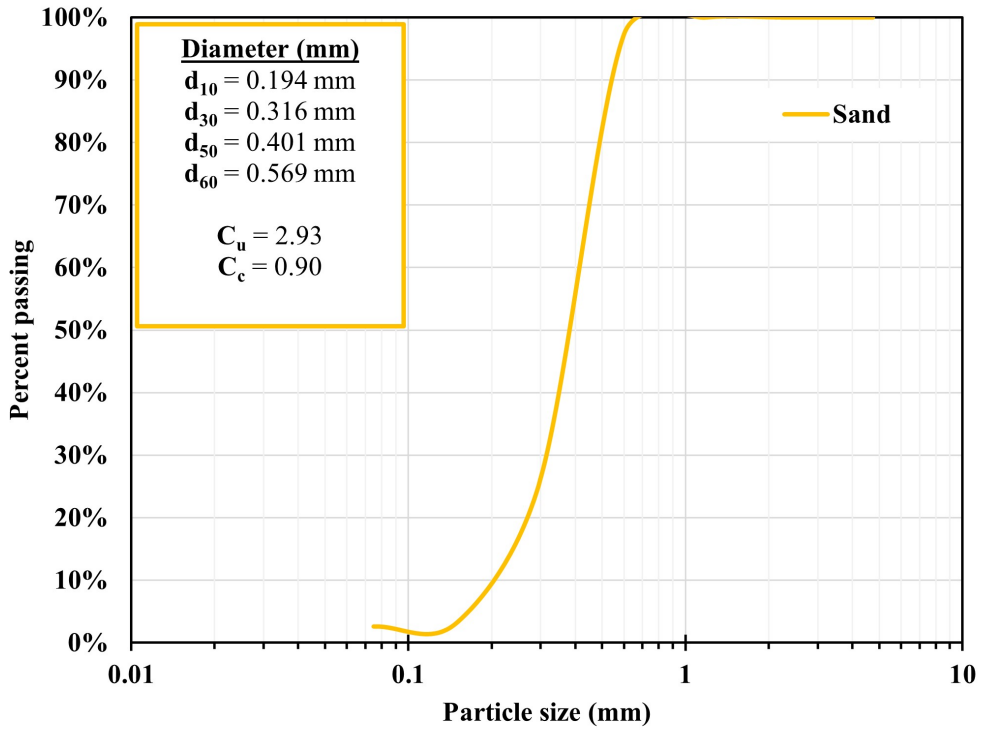

the substitution ratio of stone wool kiln ash with slag, which ranged between 10 and 30 by weight of the total binder weight (S90-W10, S80-W20, S70-W30). The reference mix, containing 100 GGBFS, was named Control. In **Table 3.**, each mix is referred to using a code name with the format Sx-Wy, where x and y represent the percentage of GGBFS and stone wool kiln ash content in the mixture. For instance, S80-W20 refers to a mortar with 80% GGBFS and 20% stone wool kiln ash as the binder. Solid pure sodium hydroxide (NaOH)(99% purity) served as the alkali activator in all formulations,added at 10% of the total weight binder for both paste and mortar mixes. The water/binder ratio was consistently set at 0.46% for both paste and mortar mixes.In mortar blends, a silica-based fine aggregate (Sika Quartz Sand 38-42) was used, and the binder/sand ratio was kept at 1:1.5. 12mm-long monofilament polypropylene microfibers (SikaFiber® PPM-12), 0.2% of the total binder weight, were used to improve durability and reduce shrinkage cracking. The physical properties of polypropylene microfiber are shown in **Table 3.2.**

Table 3.3: *Mix design composition of mortar mixes*

Mix code	GGBFS(g)	Stone wool(g)	NaOH(g)	Water(g)	Sand(g)	Fiber(g)
Control	1200	0	120	552	1800	2.4
S90-W10	1080	120	120	552	1800	2.4
S80-W20	960	240	120	552	1800	2.4
S70-W30	840	360	120	552	1800	2.4

The mixing procedure of one-part NaOH-activated GGBFS/stone wool kiln ash-based geopolymer mixes is shown in **Figure 3.3**. Firstly, binders, slag, and W20 were mixed for 30 seconds at 140 rpm using a planetary Hobart mixer. Then, the solid alkali activator NaOH was added and mixed for a further 2 minutes until the dry mixture attained a uniform color. Following this, water was added and mixed for 30 seconds. After this, the mixer was stopped, and the walls and the bottom of the mixing bowl were scraped by using a scraper to ensure all dry materials had come into contact with the water. Then, sand and fiber were first mixed homogeneously in the sample preparation stage, and then added gradually in 30 seconds and mixed for an additional 1 minute at 285 rpm when all the sand and fiber were added to the mix. Before pouring the fresh mix into the molds, the interior walls of the molds were coated with mold oil to facilitate the placement of fresh mix inside and ensure easier demolding afterward. Subsequently, the fresh mix was poured into the molds in two layers, with each layer compacted using a tampering apparatus. The molds were then covered with cloth and left in a humid cabinet for 24 hours before being demolded the following day. Finally, the samples were cured in the same humid cabinet at a temperature of 23±1°C and a relative humidity of 65 ± 5%."

3.3 Methods

3.3.1 Flowability

The flowability of geopolymer mortars was determined in accordance with the American Society for Testing and Materials (ASTM) C1437-07 standard. This test was conducted immediately following the mixing process. Specifically, the flow of the mortar

Figure 3.3: *Sample preperation of one-part geopolymer and flowchart of the experimental process*

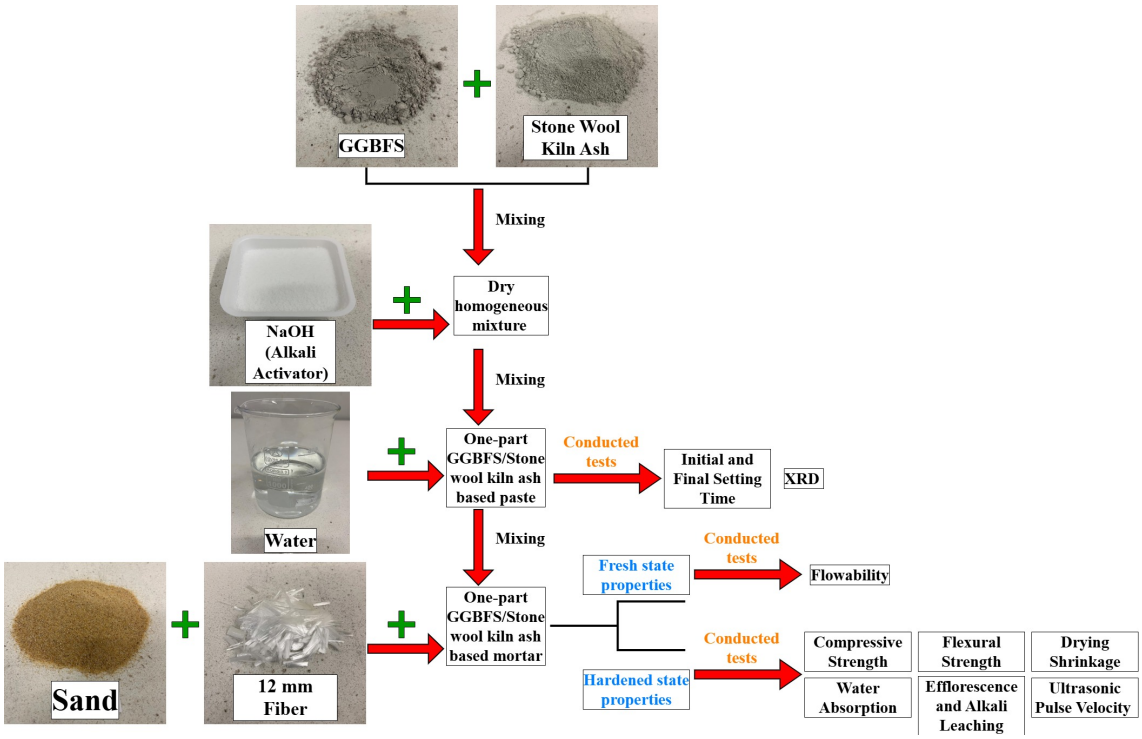

was measured by the spread of fresh mortar pulled out of a cone with a top diameter of 70 mm, a bottom diameter of 100 mm, and a height of 50 mm. After mixing, the conical mold was filled with fresh mortar in two layers. Each layer was tamped 20 times, and the excess material was cleaned off from the top of the cone. The fluidity mold was lifted off vertically,and the flow table was immediately dropped 25 times in 15 seconds. After 25 blows, the spread diameter was recorded. Four measurements were performed for each mix, and the average value and the standard deviation were reported.

3.3.2 Initial and final setting time

The initial setting times of the geopolymer paste mixes were determined by using a Vicat apparatus in accordance with the ASTM C191 standard test method. The Vicat needle test measures the depth penetrated by the needle, which indicates the resistance to axial force. The paste samples were placed into the conical ring, and the penetration depth of the Vicat needle was measured at 5-minute intervals. Based on the hydration and hardening, the penetration depth is reduced. Herein, the penetration depths of 25 mm and 0.5 mm indicate the initial and final setting times, respectively. A glass bottom plate was used and glued to avoid leakage of the geopolymer paste. The specimen was kept in a humid cabinet during testing. The testing temperature was 23±1°C, and the relative humidity was 65±5%. The average of the three samples was finally calculated as the initial and final setting time.

3.3.3 Mechanical properties

The mechanical performance of the samples was evaluated using an electromechanical universal hydraulic testing machine (UTEST Material Testing Equipment, Turkey) following EN 196-1:2016. A total of six beam specimens were cast by a triple-connected beam mold with dimensions of 40 mm×40 mm×160 mm for this experiment. The specimens were cured in a humid cabinet (temperature 23±1°C, relative humidity 65±5%) until

the testing day. Three beam specimens were used to determine the 7-day flexural strength, and another three beams were used to determine the 28-day flexural strength. The flexural strengths were determined by using a three-point bending machine with a span distance of 100 mm. The flexural strength was calculated based on Eq. **(3.1)**

$$F_f = \frac{PL}{bd^2} \tag{3.1}$$

where F_f is the specimen's flexural strength (MPa), P is the maximum applied load of the specimen fracture, and L, b, and d are the specimen's span length(mm), width(mm), and thickness(mm), respectively. The fractured portions of the specimens in a flexural strength test were placed into a 40 mm×40 mm compressive apparatus to determine the compressive strength. The compressive strength testing was carried out after curing the specimens for 7,14,28 and 56 days. The compressive strength was calculated based on Eq. **(3.2)**.

$$F_c = \frac{P}{A} \tag{3.2}$$

where F_c is the compressive strength (MPa) of the specimen, P is the maximum load applied to the specimen, and A is the area of loaded surface (mm^2).

3.3.4 Ultrasonic pulse velocity (UPV) method

A portable ultrasonic testing instrument (Controls Ultrasonic Pulse Velocity Tester) was utilized to test the UPV. This method involves measuring the travel time of ultrasonic waves over a known distance. This method was performed on 40 mm×40 mm×160 mm prism specimens right before the flexural strength test. Vaseline was utilized as a coupling agent to improve the contact between the surface of the specimen and the transducer or receiver. The transducer and receiver were placed securely against the two opposing sides of the specimen until a consistent transit time was observed. Herein, the pulse velocity was obtained by dividing the specimen length (160 mm) by the time-lapse shown in Eq. **(3.3)** and expressed in m/s. The UPV testing was performed at 7 and 28 days at room

temperature (around 23±2°C and 50 ± 5% RH). Three specimens were tested for each measurement, and the average was recorded.

$$V(x,t) = \frac{x}{t} \tag{3.3}$$

where the UPV value is represented as V(x, t), a function of the distance (x) and transit time (t).

3.3.5 Drying shrinkage and mass loss

The drying shrinkage test method in this study was employed a standard triple-connected drying shrinkage mold (50*50*200 mm)equipped with holes at both ends for reserved steel nails (6*25 mm).After casting, the specimens were cured in a humid cabinet (temperature 23±1°C, relative humidity 65±5%) for 24 hours.The initial length (L_o) and mass (M_o) of each sample was measured and recorded after 24 hours and then continued to cured in the humid cabinet in the same conditions. The digital micrometer-equipped comparator has a minimum range of 0.001 mm, while the digital electronic balance has a minimum range of 0.01 g.The measurements of drying shrinkage and mass loss were taken on days 1, 3, 7, 14, 28,56 and 90. L_t was denoted for drying shrinkage and M_t for mass loss for that specified day. Three specimens were tested for each measurement, and the average was calculated. Change in length and mass loss of the mortar were calculated using the below formulas. (Note: the steel nails is embedded in the specimen).

$$\text{Length Change}(\%) = \left(\frac{L_o - L_t}{200}\right) x100 \tag{3.4}$$

$$\text{Mass Loss}(\%) = \left(\frac{M_o - M_t}{M_o}\right) x100 \tag{3.5}$$

3.3.6 Water absorption

The water absorption test was performed on 50 × 50 × 50 mm three cube samples for each mix and kept in a humid cabinet at 23±1°C and 65 ± 5% relative humidity for

28 days. The initial mass of the geopolymer mortar specimens were recorded as (W_i). After 28 days of curing, geopolymer mortar specimens were oven-dried for 24 hours at 105°C and the mass of dried geopolymer mortar specimens wwere recorded and denoted as (W_d). Afterward, the specimens were subjected to water immersion for 48 hours. The mass of the soaked geopolymer mortar specimens was then measured and denoted as (W_w). The percentage of water absorption was measured by using three samples, and an average value was taken.

$$\text{Water absorption}(\%) = \left(\frac{W_w - W_d}{W_d}\right) x100 \tag{3.6}$$

3.3.7 Efflorescence and alkali leaching

To assess the severity of efflorescence, three beam samples of dimensions 40*40*160 mm were cast and placed in a humid cabinet at 23±1°C and 65±5% relative humidity for 28 days. After the curing period of 28 days, the samples were subjected to efflorescence conditions for an additional 28 days. Half of the depth of each sample (2 mm) was immersed in 1 liter of distilled water, while the remaining upper part of the sample was left open in ambient conditions (23±2°C and 50 ± 5% RH) until all the water was evoporated. Afterwards, the leaching products were carefully scraped from the specimens and weighted.

3.3.8 XRD analysis

A geopolymer paste specimens for each mix were prepared for XRD analysis. At 28 days, firstly, geopolymer paste samples were broken with a hammer, and crushed pieces were ground into fine powder that passed through a 300-mesh sieve. 1.5 g of the powder sample passed through the sieve was taken for XRD measurement. The Bruker D8 Discover (operated at 40 mA applied current and 40 kV accelerating voltage) was used for the XRD test. Data was collected over a 2θ range of 10° to 80° with a step size

of 0.02°.

4. RESULTS AND DISCUSSIONS

4.1 Flowability

The effect of stone wool kiln ash content in flow diameter of mortar mixes immediately after mixing, as well as the percentage flow loss is shown in **Figure 4.1.**The experimental findings clearly revealed that the increase in stone wool kiln ash content negatively affected the flowability of one-part slag/stone wool kiln ash based geopolymer samples. The Control sample has an average flow diameter of 217 mm, serving as the reference with 0% flow loss. When 10% of the slag is replaced with stone wool kiln ash (designated as S90-W10), the flow diameter decreases slightly to 212 mm, resulting in a flow loss of 2%. A more significant reduction in flow diameter occurs at 20% replacement (S80-W20), where the flow diameter drops to 187 mm, leading to a 14% flow loss. At 30%replacement (S70-W30), the flow diameter further declines to 170 mm, indicating a substantial flow loss of 21%. This is because of the stone wool kiln ash's highly porous microstructure and its significant water absorption properties [63]. This made the stone wool kiln ash function like a spongy material. The high water absorption capacity of stone wool kiln ash reduced the amount of free water present in the mix, leading to lower workability and a smaller flow diameter. In addition, the results made it possible to conclude that higher stone wool kiln ash concentration decreases the fluidity of the mixture by increasing the viscosity,means the mix becomes thicker and more resistant to flow, which is another factor that can further reduce the flow diameter.

4.2 Initial and final setting time

The initial and final setting times of the geopolymer paste made with various percentages of stone wool kiln ash replacement were measured using the Vicat needle test, with the results presented in **Figure 4.2.** As it can be seen, the replacement of slag with stone wool kiln ash significantly increased the both initial and final setting times. The

Figure 4.1: *Average flow diameter values of mortar mixes*

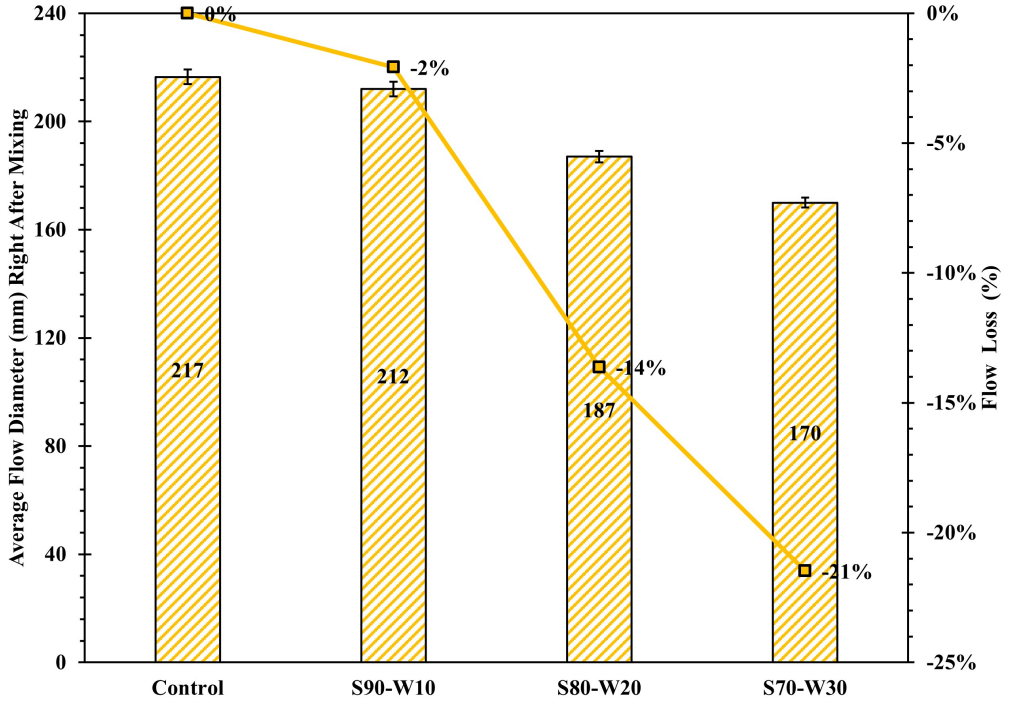

initial and final setting times of the Control mix were 19 and 24 min, respectively. The reason is that high calcium content in GGBFS precursor facilitates the formation and precipitation of calcium silicate hydrate (C–S–H) at nucleation sites, thereby promoting the rapid development of the geopolymer gel [64, 65]. For the S90-W10 mixture, the initial and final setting times are 44 minutes and 57 minutes, respectively. In contrast, the S80-W20 mixture shows increased setting times of 100 minutes for the initial setting and 134 minutes for the final setting. The S70-W30 sample, which has the highest replacement ratio, displays the slowest setting times, with an initial setting time of 204 minutes and a final setting time of 258 minutes. A comparable behavior was observed when stone wool kiln ash was incorporated into cement [66], supporting the conclusion that stone wool kiln ash exhibits no hydraulic activity. Herein, the findings indicate that the concentration of NaOH improved the dissolution of stone wool kiln ash particles, leading to a significant release of silicon and aluminium ions, while the concentration of calcium in the solution

decreased. As a result, the dissolution process took longer to complete, which in turn extended the geopolymerization reaction time and increased the both initial and final setting time [22].

Figure 4.2: *Initial and final setting of geopolymer paste*

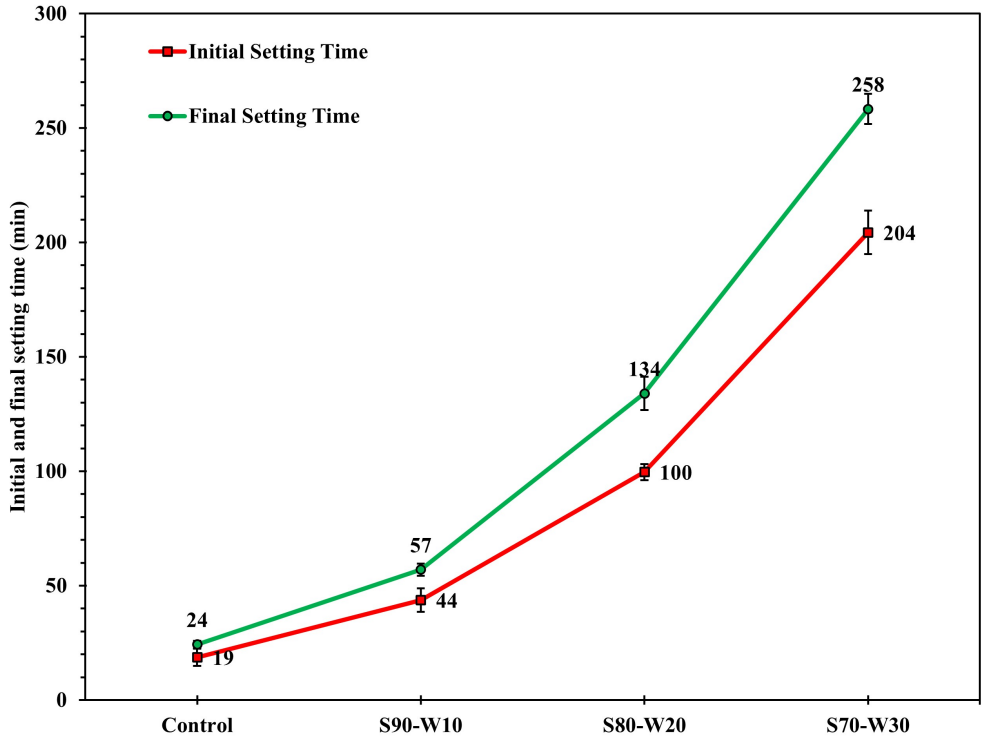

4.3 Mechanical properties

The flexural strengths at 7 and 28 days are shown in **Figure 4.3.** The flexural strengths of all specimens (except S80-W20 and S70-W30) increased with increasing curing time from 7 to 28 days, owing to further geopolymerization reaction. The Control sample exhibits a flexural strength of 2.7 MPa at 7 days and 3.0 MPa at 28 days, reflecting a 12% increase over time. The S90-W10 mixture shows a significant improvement in flexural strength, reaching 3.9 MPa at 7 days and 4.6 MPa at 28 days, which corresponds to a 20% strength gain. In contrast, the S80-W20 mixture demonstrates a slight decrease in flexural strength, showing a 5% reduction with values of 4.8 MPa at 7 days and 4.5

Figure 4.3: *Flexural strength results of mortar mixes at 7 and 28 days*

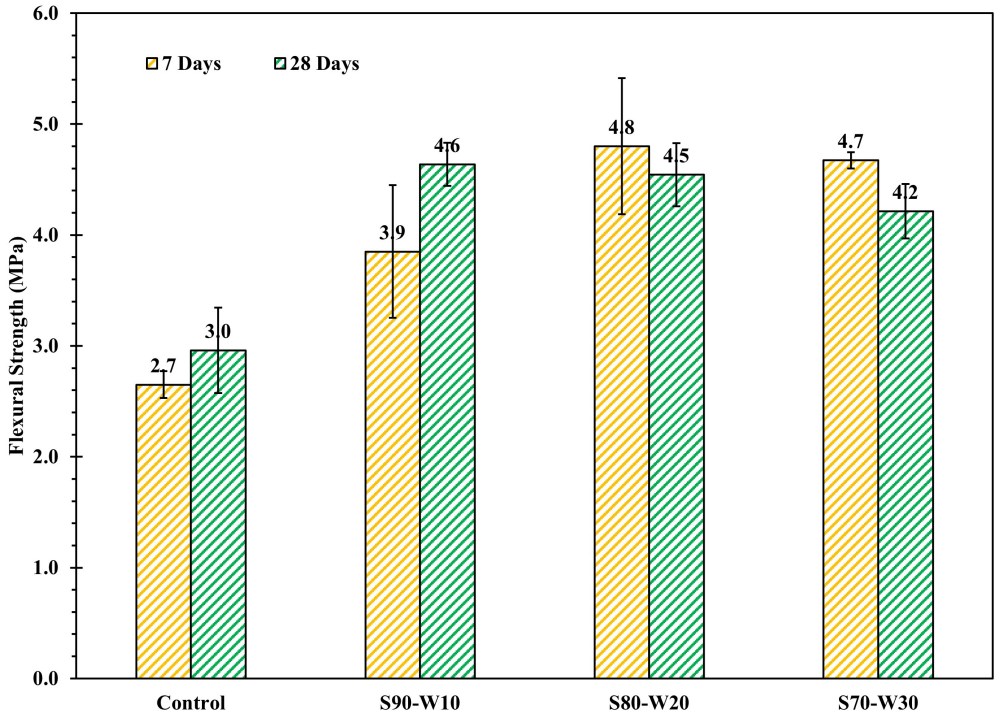

MPa at 28 days. Notably, the S70-W30 mixture presents a more pronounced decline in strength over time, with flexural strength values of 4.7 MPa at 7 days and 4.2 MPa at 28 days, representing a 10% reduction. Overall, it can be stated that flexural strength increases initially and then stabilized at higher stone wool kiln ash replacement levels. 10% of stone wool kiln ash filled voids between grains, leading to a denser microstructure and enhanced mechanical properties. Previous studies have shown that an increase in the Ca/Si ratio and a decrease in the Al/Si ratio contribute to enhanced material strength [67].The incorporation of stone wool kiln ash increases the silica content in the system while reducing the Al/Si ratio, resulting in more Si-O-Si bonds and further strengthening the material.

The **Figure 4.4** presents the compressive strength development of mixtures with varying stone wool kiln ash contents, measured at 7, 14, 28, and 56 days. The control sample achieves compressive strengths of 27.0 MPa, 33.7 MPa, 41.6 MPa, and 44.5 MPa at

7, 14, 28, and 56 days, respectively, showing a steady increase over time. Replacing 10% of slag with stone wool kiln ash (S90-W10) significantly enhances compressive strength, reaching 37.0 MPa, 49.2 MPa, 50.3 MPa, and 53.2 MPa at the respective curing intervals. The main reason is that the SiO_2 / Al_2O_3 ratio in the geopolymer also rises, facilitating the formation of more complex silico-aluminate gel structures, which in turn enhances the compressive strength of the geopolymer mortar [68]. Similar to the flexural strength results, compressive strength showed an increasing and decreasing trend with increasing stone wool kiln ash content. After 10% addition of stone wool kiln ash replacement, this positive trend however began to drop. At 20% replacement (S80-W20), the compressive strength values are slightly lower at 33.4 MPa, 43.5 MPa, 42.5 MPa, and 44.8 MPa for the same intervals, indicating reduced strength enhancement with higher ash content. Finally, the S70-W30 mixture (30% replacement) shows the lowest compressive strength values of 25.2 MPa, 30.8 MPa, 31.9 MPa, and 36.2 MPa. The compressive strength of geopolymer mortar decreased when a high content of stone wool kiln ash was used. This could be attributed to the formation of weak and porous structures of stone wool kiln ash within the matrix, rather than a dense gel formation. In an alkaline environment, some particles of stone wool kiln ash undergo partial decomposition and fail to participate in the reactions. As a result, fewer reaction products are formed, leading to a reduction in strength [2].

4.4 UPV method

The variation in ultrasonic pulse velocity of geopolymer mortar, measured at 7 and 28 days, for different stone wool kiln ash content is presented in **Figure 4.5.** The Control sample exhibits the highest UPV values of 3675 m/s and 3684 m/s at 7 and 28 days, respectively. These values reflect a dense and well-structured matrix. When 10% stone wool kiln ash is introduced (S90-W10), the UPV values decrease slightly to 3481 m/s for both testing periods, indicating minimal disruption to the geopolymer structure.

Figure 4.4: *Compressive strength results of mortar mixes at 7,14,28 and 56 days*

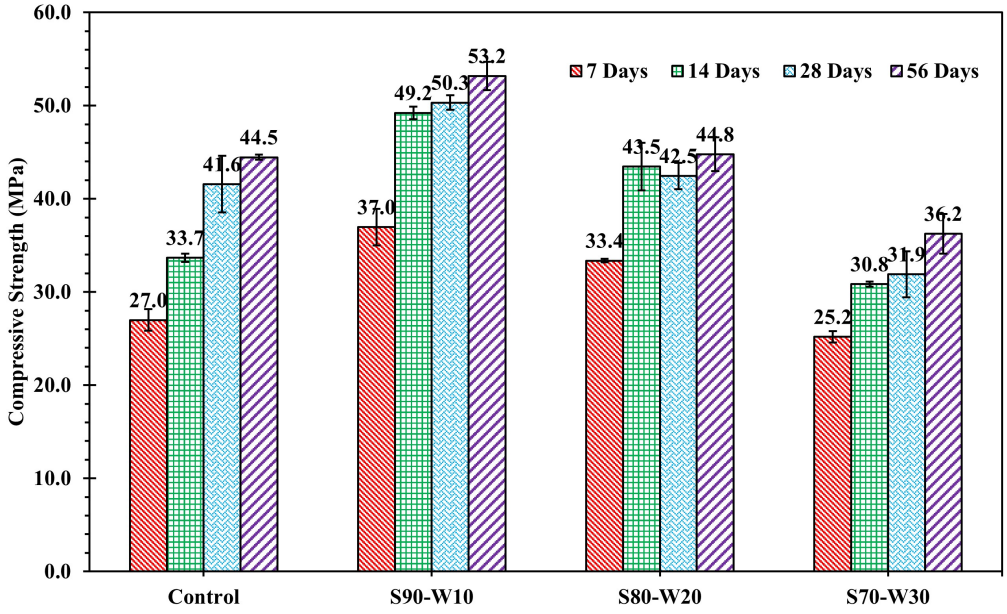

However, increasing the ash content to 20% (S80-W20) results in a more significant drop in UPV, with values of 3118 m/s at 7 days and 2951 m/s at 28 days. This decline suggests a reduction in matrix integrity and an increase in porosity. The sample with the highest ash content (S70-W30) records the lowest UPV values of 2807 m/s and 2799 m/s, highlighting a significant deterioration in the geopolymer structure due to the excessive substitution of slag with stone wool kiln ash. According to BIS 13311-1:1992 [69], when the UPV values range between 3500 m/s and 4500 m/s, the concrete is categorized as ”good concrete.” If the UPV values between 3000 m/s and 3500 m/s, the concrete is classified as being of medium quality. The below 3000 m/s is named as doubtful. The addition of stone wool kiln ash increases the porosity of the geopolymer matrix, leading to a decrease in wave velocity. As can be observed that the pulse velocity of geopolymer mortar decreased from 3684 m/s to 2799 m/s over a 28 day period as the percentage of stone wool kiln ash was increased from 0% to 30% as a partial substitute for GGBFS. This indicates that higher amounts of stone wool kiln ash negatively impact the quality and homogeneity of the mortar. This decline trend was also aligned in decreasing the compressive strength results

(**Figure 4.4.**).

Figure 4.5: *UPV results of mortar mixes*

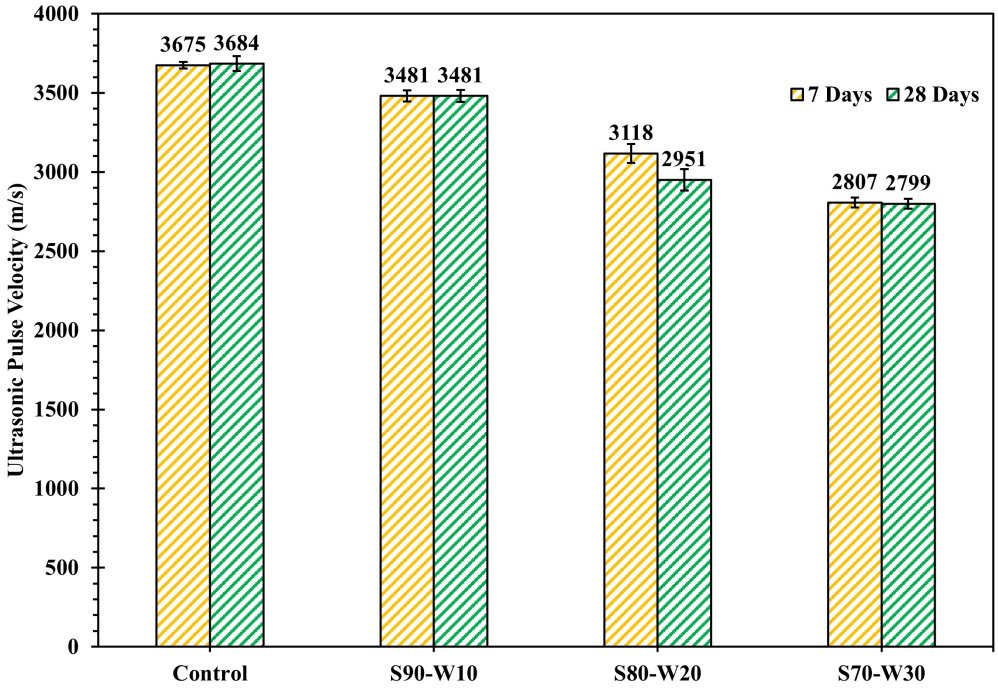

4.5 Drying shrinkage and mass loss

Figure 4.6 illustrates the impact of different stone wool kiln ash contents on the percent length changes in slag-based geopolymer mortar. Based on the results, increasing the stone wool kiln ash resulted in a higher degree of length change. At 90 days, the length change rates for groups Control, S90-W10, S80-W20, and S70-W30 were 0.52%, 0.71%, 0.88%, and 0.95%, respectively. Geopolymers experience shrinkage under drying conditions due to water evaporation from gel and capillary pores [70, 71]. Unlike OPC, geopolymers contain a significant amount of interstitial water, rather than chemically bound water, within their matrix [71]. As a result, the capillary stress between the dry and wet regions of the capillary pores becomes relatively high due to the evaporation of a substantial amount of non-chemically bound water [72, 16]. As shown in the **Figure 4.6**, the drying shrinkage rate of slag-based geopolymers increases rapidly during the first

seven days as the stone wool kiln ash content rises, followed by a slower growth phase. By 56 days of curing, the shrinkage rate was stabilized except the Control sample, suggesting that the early-stage geopolymerization and hydration reactions in the slag-based system are initially intense but gradually subside after the 56-day curing period [73]. Additionally, an increase in stone wool kiln ash content leaded to elevated tensile stress within the capillary pores, consequently amplifying the drying shrinkage rate [74].

Figure 4.6: *Length change in specimen with respect to time*

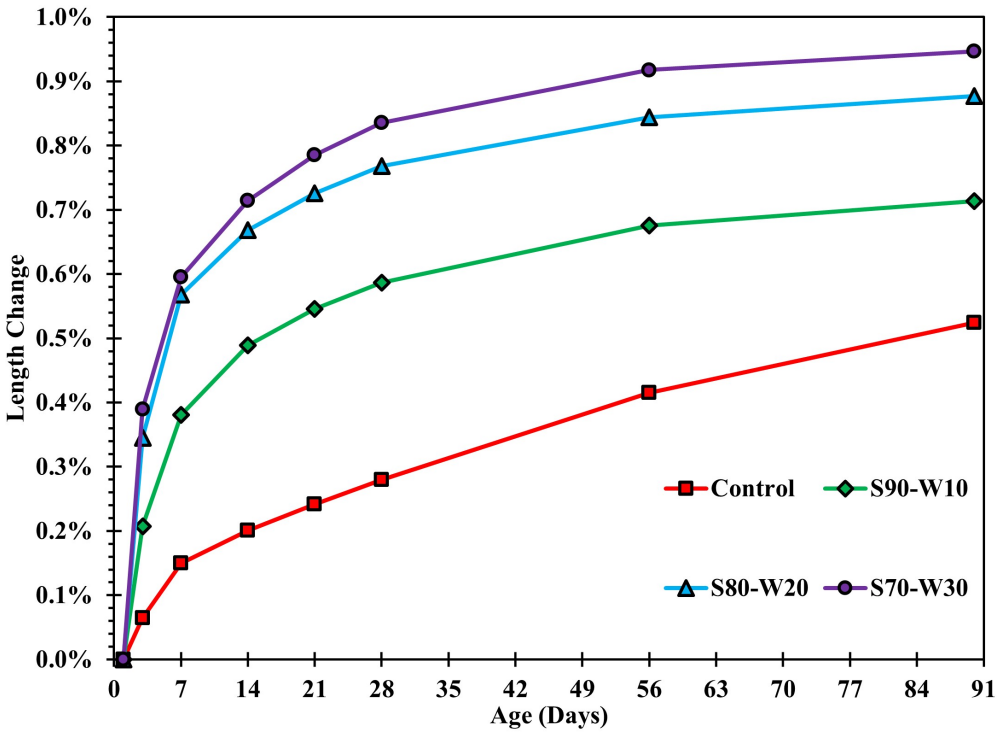

Furthermore, **Figure 4.7** presents the variation in mass loss rates for geopolymer mixtures at differing stone wool kiln ash content, showing a clear increase in mass loss as stone wool kiln ash content rises. Specifically, at 90 days, the mass loss rates for groups Control, S90-W10, S80-W20, and S70-W30 were 2.4%, 2.1%, 3.0%, and 4.1%, respectively. Once drying begins, mass loss proceeded rapidly during the initial days before stabilizing and eventually reaching a nearly constant value.Moreover, the majority of the mass loss occurred within the first seven days after the drying process began. A

significant increase in mass loss is observed when the stone wool kiln ash content is at 30%. Notably, after 28 days, it was observed that the mass loss in S90-W10 was lower than in the Control sample. This observation indicates that incorporating 10% of stone wool kiln ash in slag-based geopolymer fosters the denser microstructure with decreasing void content, slowing down the mass of geopolymer mortar. Additionally, this reduces water evaporation, which in turn lowers the capillary stress [75]. This greater mass loss in compositions with higher stone wool kiln ash content can be attributed to the finer particles and pore structure of the stone wool kiln ash, which enhances water adsorption.As a result, the increased water absorption intensified the shrinkage effect caused by water evaporation [73].

Figure 4.7: *Mass loss in specimen with respect to time*

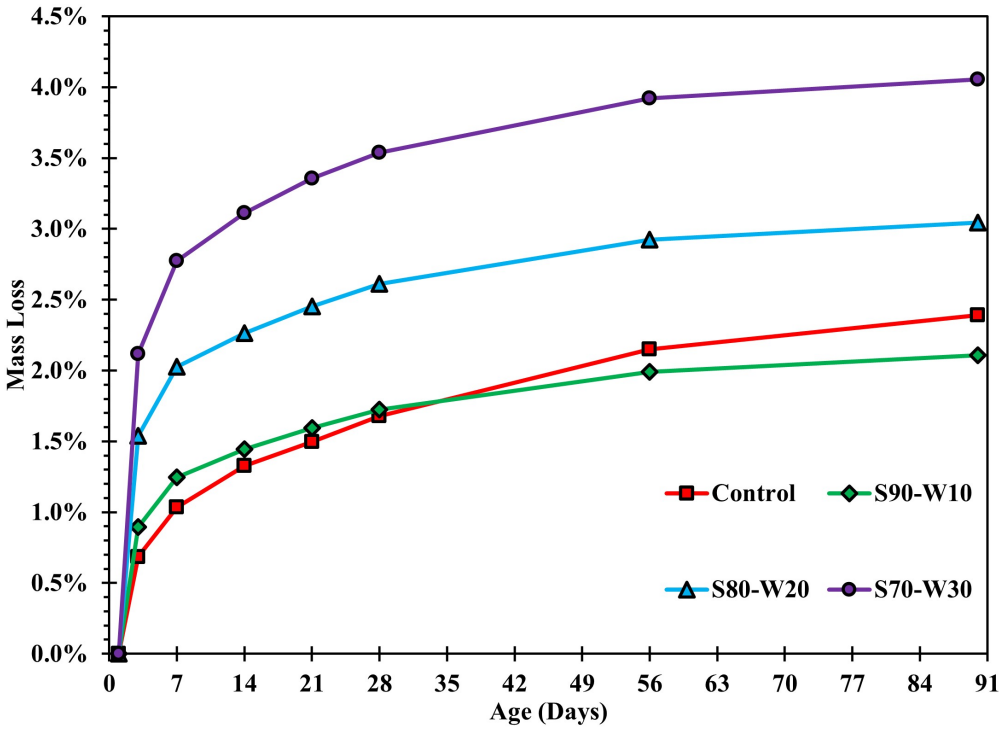

Last but not least, **Figure 4.8** represents the density changes of geopolymer mortar samples over 90 days. The Control sample maintains the highest density, beginning at approximately 2.21 g/cm³ and stabilizing near 2.16 g/cm³ by day 90. With 10% stone

wool kiln ash replacement, the initial density is drastically decreased from 2.21 g/cm³ to 2.13g/cm³ compared to the Control sample and stabilizes at approximately 2.08 g/cm³. When the stone wool kiln ash content continued to increased, the geopolymer mortar's initial density drastically decreased. The initial density of S80-W20 and S70-W30 were 2.11 g/cm³ and 2.10 g/cm³ and stabilizing near 2.05 g/cm³ and 2.02 g/cm³ by day 90. Moreover, it has to be noted that the highest loss occurred in the first three days. This is because of free water evaporate from the pore structure of the matrix efforlessly, leading to decrease the weight of the mortar. This proved that stone wool kiln ash has a porous structure.

Figure 4.8: *Changing of density with respect to time*

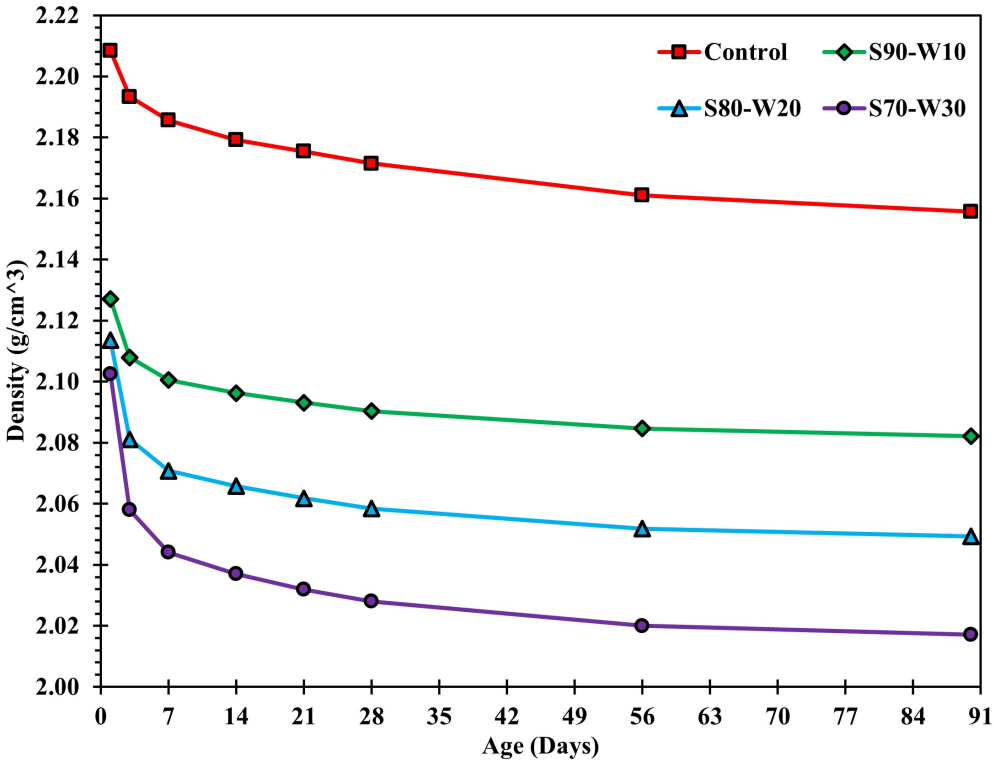

Based on the length change and mass loss data presented in **Figure 4.9**, the study also examined the relationship between the experimentally measured length change and mass loss. The analysis demonstrated a strong correlation between these parameters, as

indicated by the R^2 value of 0.79 for the fitting curve. The slope (0.25) suggests that for each 1% decrease in mass loss, the shortening of the specimen was approximately 0.25%. This relationship highlights that as mass loss increases, the geopolymer mortar also exhibits more significant dimensional changes. This result suggests that the drying shrinkage of slag-stone wool kiln ash-based geopolymer is primarily driven by water evaporation. Specifically, variations in drying shrinkage are likely associated with changes in the distribution and connectivity of the pore structure and the amount of water available for evaporation.

Figure 4.9: *Length change vs. mass loss fitting curve*

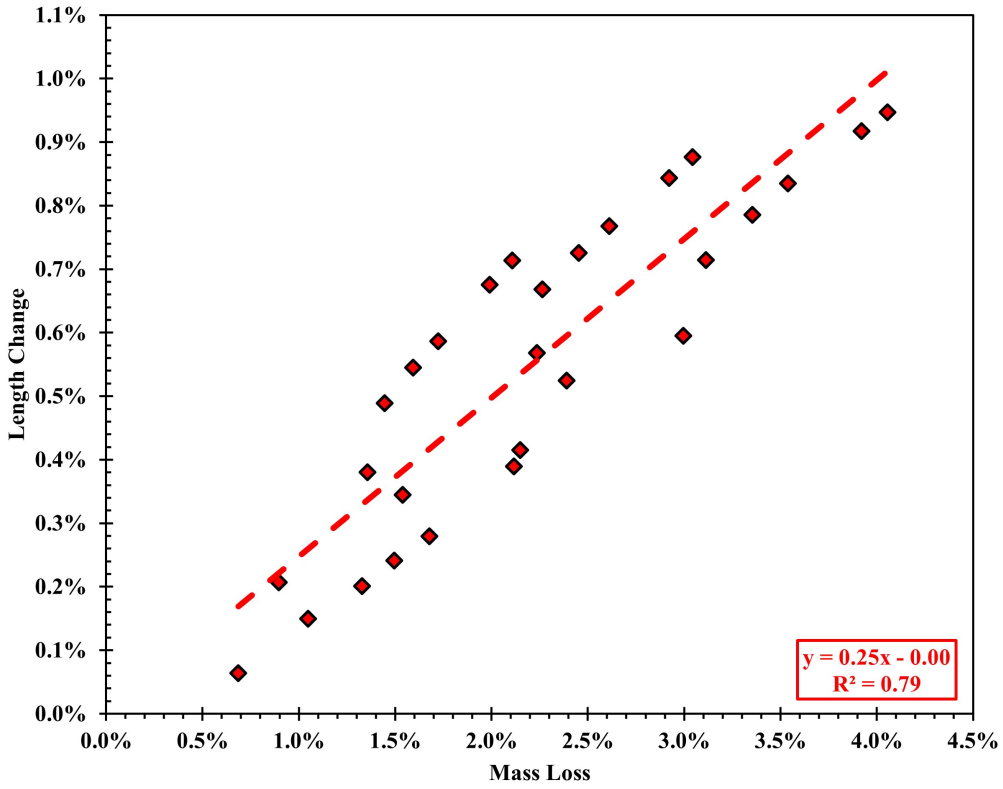

4.6 Water absorption

Incorporating stone wool kiln ash in geopolymer mortar was affected the water absorption characteristics. **Figure 4.10** shows the water absorption percentages for geopolymer mortars. The control mix exhibited the lowest water absorption of 8.44%. However, as the stone wool kiln ash content increased from 10% (S90-W10) to 30% (S70-W30), the water absorption values increased significantly to 8.63%, 8.82%, and 9.10%, respectively. This trend reveals that the higher content of stone wool kiln ash decreased the proper packaging of the matrix, leading to increased capillary pores in the mixture and resulting in a looser microstructure and interfacial transition zone, causing increased water absorption. Another reason could be the excessive amount of stone wool kiln ash, which slowed polycondensation reactions and generated gaps following the evaporation of unreacted water molecules, resulting in increased water absorption. Also, higher water absorption typically indicates increased porosity, which compromises the density and integrity of the material matrix [76]. When water penetrates the geopolymer mortar, it occupies voids within the structure, reducing the overall compactness and leading to a weaker bond between aggregates and the geopolymer paste. This weakened structure directly reduces the material's ability to withstand compressive loads, which also aligns with the compressive strength results (**Figure 4.4**). This suggests that the water absorption test could potentially serve as a reliable indirect indicator for evaluating the performance of geopolymer samples.

4.7 Efflorescence and alkali leaching

The connection between alkali leaching and compressive strength in geopolymer mortar is crucial; increased alkali leaching significantly reduces compressive strength[16].

Figure 4.10: *Water absorption of geopolymer mortars*

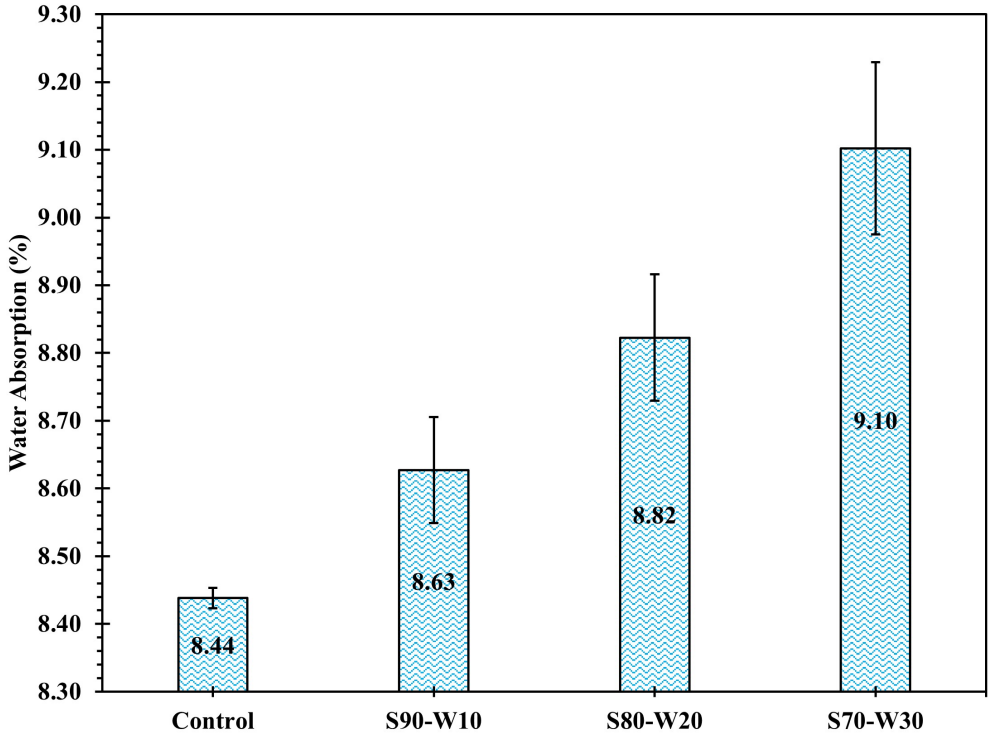

When exposed to water or harsh environments, alkali leaching occurs [77], losing of important alkali ions like sodium and potassium from the material. This detrimental process raises porosity and compromises the matrix's structural integrity, creating voids that weaken the mortar. This behavior was categorized by Zhang et al. [78] as sub-florescence, which occurs due to the crystallization of carbonates within the pore structure of the near-surface layer. This crystallization induces stress, leading to cracking and the deterioration of the material. The **Figure 4.11.** demonstrates the relationship between compressive strength and total leaching amounts for geopolymer mortars. The Control sample shows a commendable compressive strength of 52.9 MPa alongside a leaching amount of 11.01 grams. Remarkably, by incorporating just 10% stone wool kiln ash (S90-W10), compressive strength was increased to 57.8 MPa, while the leaching amount substantially drops to 9.46 grams. This improvement signifies a denser microstructure and fewer voids, enhancing overall integrity.As the ash content increases to 20% (S80-W20), the compressive

strength decreases to 50.2 MPa, while the leaching amount rises to 11.02 grams. This suggests that higher stone wool kiln ash replacement can produce porous microstructure with connected pores, facilitating the movement of water and free alkalis to the surface and promoting the formation of efflorescence. Same phenomeneon was also observed at the highest ash content of 30% (S70-W30), the compressive strength further declines to 41.0 MPa, and the leaching amount increases to 11.2 grams.

Figure 4.11: *Relationship between compressive strength and total leaching amount*

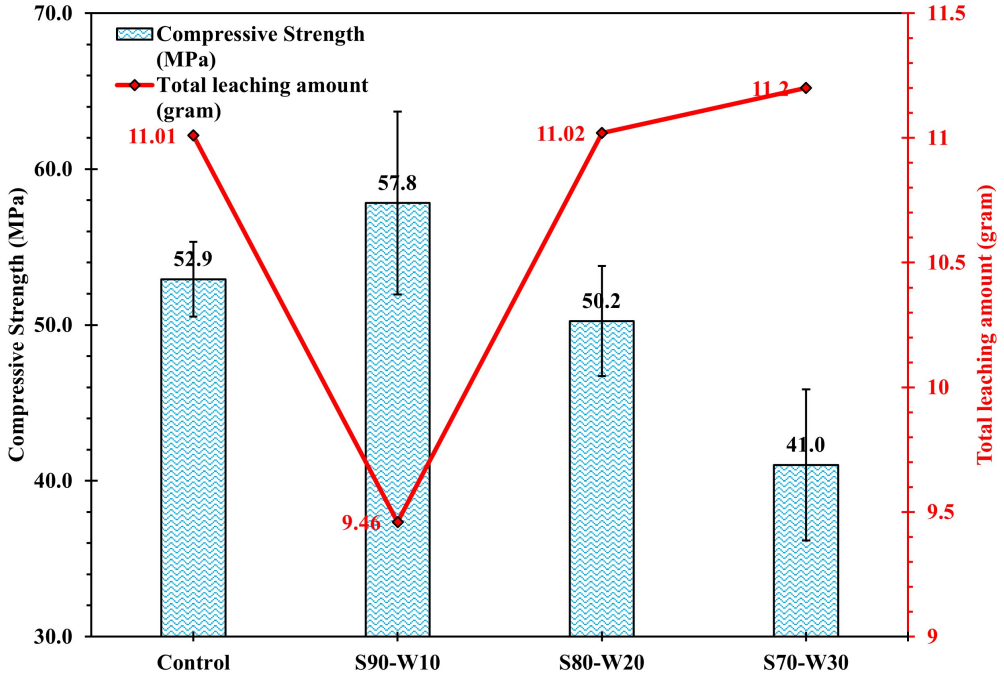

4.8 XRD analysis

Figure 4.12. shows the XRD pattern of the paste geopolymer after 28 days. As can be observed, the amorphous hump observed at 2θ = 20–35° in all geopolymers represented the amorphous aluminosilicate gel in the geopolymer, which was one of the primary phases of the geopolymer[79, 80]. As the stone wool kiln ash content increases (from S90-W10 to S70-W30), the intensity of the amorph peaks becomes more pronounced. This suggests that stone wool kiln ash affects the amorph phases. Notable

peaks at 2θ [81, 79] are probably associated with calcite ($CaCO_3$) phases. The decrease in the amorphous hump with an increase in the content of stone wool in the kiln ash indicates a reduction in the amorphous geopolymer gel, which is linked to the decrease in mechanical properties shown in **Figure 4.4.**. Furthermore, the slight broadening of some peaks in samples with higher stone wool kiln ash content (e.g., S70-W30) suggests destruction of matrix structure, likely due to interactions between the GGBFS and stone wool kiln ash during the geopolymerization process. **Figure A.7** in the Appendices section shows the core structure of geopolymer paste at 28 days and it is evident that the gel formation was reduced when the stone wool kiln ash increases.

Figure 4.12: *XRD analysis of geopolymer paste specimens at 28 days*

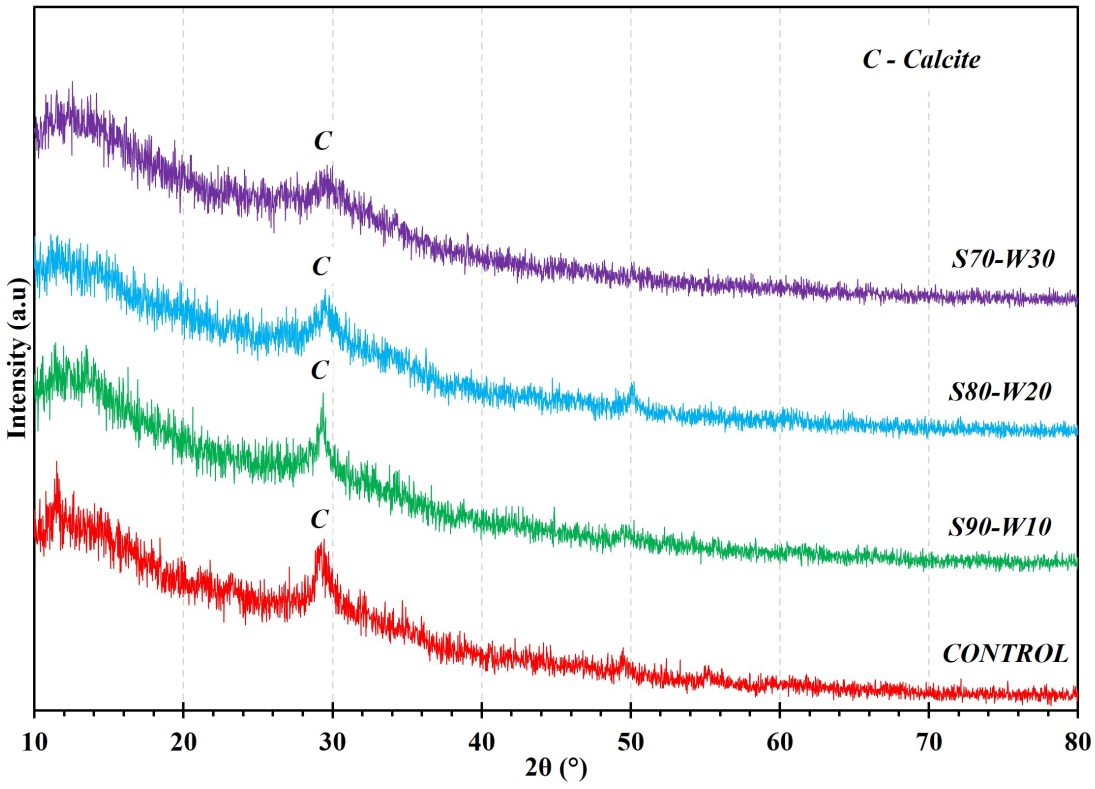

5. CONCLUSIONS

This thesis evaluated the effect of incorporating stone wool kiln ash as a part precursor in one-part slag-based geopolymer mortars with sodium hydroxide as the activator. 4 different mix design compositions were considered, and the fresh and hardened properties and the microstructure of the mixes' microstructure were investigated. Based on the test results, the following conclusions were drawn:

- The workability of fresh mortar decreases significantly as the stone wool kiln ash content increases. This reduction can be attributed to the higher water absorption capacity of stone wool kiln ash than slag. Additionally, the porous structure of stone wool kiln ash particles raises water demand, contributing to reduced workability.

- Both initial and final setting time increases significantly as the stone wool kiln ash content increases. This was due to the high amount of SiO_2 in stone wool kiln ash, resulting in a slower reaction and formation of C-S-H gel in the early stages, thereby extending the setting time.

- The mix comprising 90% slag and 10% stone wool kiln ash (S90-W10) exhibited the highest flexural and compressive strengths among all formulations, exhibiting 4.6 and 50.3 MPa at 28 days. Higher the stone wool kiln ash replacement adversly affect the mechanical properties. This decline is due to the weaker products formed during the dissolution of stone wool kiln ash particles compared to the activation products of slag. Additionally, a higher proportion of stone wool kiln ash leads to an increased number of unreacted particles, resulting in a less dense microstructure and further reducing the strength.

- The impact of stone wool kiln ash content on the percentage of length change and

mass loss in one-part geopolymer mortar exhibits a similar trend. A linear relationship is observed between these two factors, which can be attributed to the evaporation of water from the mortar pores. This evaporation causes both mass loss and drying shrinkage. Thus, reducing water evaporation or decreasing the quantity of evaporation water in the pores is an effective strategy to address the issue of drying shrinkage.

- The higher alkali leaching products were obtained when the stone wool kiln ash content increased. The increased alkali leaching is generally associated with durability issues and a decline in compressive strength. Excessive stone wool kiln ash content disrupted the balance of the geopolymerization process, potentially leading to incomplete gel formation, and this weakened the microstructure, resulting in decreased compressive strength as observed.

- The results from water absorption, UPV, and XRD tests demonstrated that higher levels of stone wool kiln ash replacement adversely affect material properties by decreasing packing density, increasing porosity, creating a looser microstructure, and reducing the homogeneity of the matrix.

- Considering all the experimental results of this study, a 10% replacement of stone wool kiln ash was determined to be the optimal ratio, significantly improving performance and material properties. Conversely, a 20% replacement was found to represent the threshold level, beyond which further replacement may negatively impact the both fresh and hardened properties.

5.1 Limitations

- **Lack of standard regulations:** There are fewer established industry standards and regulations for geopolymer concrete compared to traditional cement-based concrete. This can make it difficult to gain acceptance in construction projects and may limit its widespread adoption.

- **High construction costs:** The high cost of alkali activators, especially sodium hydroxide, can make the material less cost-effective than traditional concrete.

- **Raw Material Availability:** The availability of raw materials such ash slag and stone wool kiln ash can be limited in some regions and the quality of these materials can also vary because of being as an waste material, affecting the performance of the final product.

5.2 Future Works

In this thesis, one-part slag-stone wool kiln ash geopolymer were investigated. However, there are several potential modifications or novel approaches that could be explored to enhance the performance of geopolymer-based materials.The following areas are recommended for further research:

- It is recommended to conduct Scanning Electron Microscope (SEM),Fourier Transform Infrared Spectroscopy (FTIR), and Thermal Gravimetric Analysis (TGA) tests to gain a deeper understanding of the surface topography, chemical compositions, and bonding mechanisms between particles.

- Rheological parameters such as static yield stress, dynamic yield stress, viscosity and thixotropy should be examined to understand the influence of stone wool kiln ash particles.

- Various materials, such as metakaolin or fly ash, can be explored as alternatives to slag. Additionally, the incorporation of nanoparticles like nano-montmorillonite or clays such as sepiolite may help to enhance the performance of geopolymer concrete.

REFERENCES

[1] J. Zhao, L. Tong, B. Li, T. Chen, C. Wang, G. Yang, and Y. Zheng, "Eco-friendly geopolymer materials: A review of performance improvement, potential application and sustainability assessment," *Journal of Cleaner Production*, vol. 307, p. 127085, 2021.

[2] P. Shoaei, A. Momenzadeh, H. Hosseini, S. Rajaei, F. Ameri, and S. Pilehvar, "One-part slag/zeolite geopolymer mortars under ambient and heat curing conditions," *Case Studies in Construction Materials*, vol. 20, p. e02677, 2024.

[3] B. Nikmehr, B. Kafle, A. W. Al Zand, and R. Al-Ameri, "The effect of hybrid basalt fibres on the mechanical and structural characteristics of geopolymer concrete containing geopolymer-coated recycled concrete aggregates," *Construction and Building Materials*, vol. 450, p. 138649, 2024.

[4] K. L. Scrivener, V. M. John, and E. M. Gartner, "Eco-efficient cements: Potential economically viable solutions for a low-co2 cement-based materials industry," *Cement and concrete Research*, vol. 114, pp. 2–26, 2018.

[5] M. Abdellatief, M. Abd Elrahman, A. A. Abadel, M. Wasim, and A. Tahwia, "Ultra-high performance concrete versus ultra-high performance geopolymer concrete: mechanical performance, microstructure, and ecological assessment," *Journal of Building Engineering*, vol. 79, p. 107835, 2023.

[6] Y. Min, M. Gao, C. Yao, J. Wu, and X. Wei, "On the use of one-part geopolymer activated by solid sodium silicate in soft clay stabilization," *Construction and Building Materials*, vol. 402, p. 132957, 2023.

[7] G. Habert, J. D. De Lacaillerie, and N. Roussel, "An environmental evaluation of geopolymer based concrete production: reviewing current research trends," *Journal of cleaner production*, vol. 19, no. 11, pp. 1229–1238, 2011.

[8] I. S. Ayeni, N. H. A. S. Lim, and M. Samad, "Engineering properties of natural fibre-reinforced one-part geopolymer concrete," *Construction and Building Materials*, vol. 456, p. 139161, 2024.

[9] B. C. McLellan, R. P. Williams, J. Lay, A. Van Riessen, and G. D. Corder, "Costs and carbon emissions for geopolymer pastes in comparison to ordinary portland cement," *Journal of cleaner production*, vol. 19, no. 9-10, pp. 1080–1090, 2011.

[10] J. Davidovits, "Geopolymers and geopolymeric materials," *Journal of thermal analysis*, vol. 35, pp. 429–441, 1989.

[11] J. Davidovits, "Geopolymers: inorganic polymeric new materials," *Journal of Thermal Analysis and calorimetry*, vol. 37, no. 8, pp. 1633–1656, 1991.

[12] B. Nematollahi, J. Sanjayan, and F. U. A. Shaikh, "Synthesis of heat and ambient cured one-part geopolymer mixes with different grades of sodium silicate," *Ceramics International*, vol. 41, no. 4, pp. 5696–5704, 2015.

[13] E. N. Kani, A. Allahverdi, and J. L. Provis, "Efflorescence control in geopolymer binders based on natural pozzolan," *Cement and Concrete Composites*, vol. 34, no. 1, pp. 25–33, 2012.

[14] W. Chen, J. Pan, B. Zhu, X. Ma, Y. Zhang, Y. Chen, X. Li, L. Meng, and J. Cai, "Improving mechanical properties of 3d printable 'one-part'geopolymer concrete with steel fiber reinforcement," *Journal of Building Engineering*, vol. 75, p. 107077, 2023.

[15] M. Yu, T. Wang, Y. Chi, D. Li, L.-y. Li, and F. Shi, "Residual mechanical properties of ggbs-fa-sf blended geopolymer concrete after exposed to elevated temperatures," *Construction and Building Materials*, vol. 411, p. 134378, 2024.

[16] Y. A. Atalay, T. Aydın, Z. B. Bundur, P. Mokhtari, M. A. Gülgün, and Z. Lafhaj, "Optimization of hybrid microwave curing approach based on the performance of metakaolin-based geopolymer mortars," *Turkish Journal of Civil Engineering*, vol. 35, no. 6, 2024.

[17] Ö. C. Özen, D. Oktay, and B. Aktürk, "One-part sodium carbonate-activated slag/r-mgo based mixes: Influence of nano-silica incorporation on compressive strength and microstructural development," *Construction and Building Materials*, vol. 422, p. 135844, 2024.

[18] M. U. Salim and C. Moro, "Towards sustainable construction: Performance evaluation of slag-cenosphere geopolymers under different naoh concentrations," *Journal of Building Engineering*, vol. 91, p. 109605, 2024.

[19] P. Duxson, A. Fernández-Jiménez, J. L. Provis, G. C. Lukey, A. Palomo, and J. S. van Deventer, "Geopolymer technology: the current state of the art," *Journal of materials science*, vol. 42, pp. 2917–2933, 2007.

[20] J. Provis and J. Van Deventer, "Geopolymerisation kinetics. 2. reaction kinetic modelling," *Chemical engineering science*, vol. 62, no. 9, pp. 2318–2329, 2007.

[21] M. Zareechian, H. Siad, M. Lachemi, and M. Sahmaran, "Advancements in cleaner production of one-part geopolymers: A comprehensive review of mechanical properties, durability, and microstructure," *Construction and Building Materials*, vol. 409, p. 133876, 2023.

[22] K. Yomthong, D. Wattanasiriwech, P. Aungkavattana, and S. Wattanasiriwech, "Effect of naoh concentration and curing regimes on compressive strength of fly ash-based geopolymer," *Materials Today: Proceedings*, vol. 43, pp. 2647–2654, 2021.

[23] S. Yaseri, G. Hajiaghaei, F. Mohammadi, M. Mahdikhani, and R. Farokhzad, "The role of synthesis parameters on the workability, setting and strength properties of binary binder based geopolymer paste," *Construction and Building Materials*, vol. 157, pp. 534–545, 2017.

[24] A. Karthik, K. Sudalaimani, and C. V. Kumar, "Investigation on mechanical properties of fly ash-ground granulated blast furnace slag based self curing bio-geopolymer concrete," *Construction and Building Materials*, vol. 149, pp. 338–349, 2017.

[25] T.-W. Cheng and J. Chiu, "Fire-resistant geopolymer produced by granulated blast furnace slag," *Minerals engineering*, vol. 16, no. 3, pp. 205–210, 2003.

[26] N. Ganesan, R. Abraham, and S. D. Raj, "Durability characteristics of steel fibre reinforced geopolymer concrete," *Construction and Building Materials*, vol. 93, pp. 471–476, 2015.

[27] M. Zhang, H. Guo, T. El-Korchi, G. Zhang, and M. Tao, "Experimental feasibility study of geopolymer as the next-generation soil stabilizer," *Construction and building materials*, vol. 47, pp. 1468–1478, 2013.

[28] K. Han, F. Gu, H. Yang, X. Tian, and X. Du, "Pva fiber reinforced red mud-based geopolymer for 3d printing: Printability, mechanical properties and microanalysis," *Journal of Building Engineering*, vol. 97, p. 110733, 2024.

[29] A. Hajimohammadi, T. Ngo, and A. Kashani, "Sustainable one-part geopolymer foams with glass fines versus sand as aggregates," *Construction and Building Materials*, vol. 171, pp. 223–231, 2018.

[30] E. Yusslee and S. Beskhyroun, "Performance evaluation of hybrid one-part alkali activated materials (aams) for concrete structural repair," *Buildings*, vol. 12, no. 11, p. 2025, 2022.

[31] O. Mahmoodi, H. Siad, M. Lachemi, S. Dadsetan, and M. Şahmaran, "Optimized application of ternary brick, ceramic and concrete wastes in sustainable high strength geopolymers," *Journal of cleaner production*, vol. 338, p. 130650, 2022.

[32] S. Dadsetan, H. Siad, M. Lachemi, O. Mahmoodi, and M. Sahmaran, "Optimization and characterization of geopolymer binders from ceramic waste, glass waste and sodium glass liquid," *Journal of Cleaner Production*, vol. 342, p. 130931, 2022.

[33] M. Pavlin, B. Horvat, A. Frankovič, and V. Ducman, "Mechanical, microstructural and mineralogical evaluation of alkali-activated waste glass and stone wool," *Ceramics International*, vol. 47, no. 11, pp. 15102–15113, 2021.

[34] O. Gencel, O. Karadag, O. H. Oren, and T. Bilir, "Steel slag and its applications in cement and concrete technology: A review," *Construction and Building Materials*, vol. 283, p. 122783, 2021.

[35] K. L. Scrivener and R. J. Kirkpatrick, "Innovation in use and research on cementitious material," *Cement and concrete research*, vol. 38, no. 2, pp. 128–136, 2008.

[36] K. Pasupathy, S. Ramakrishnan, and J. Sanjayan, "3d concrete printing of eco-friendly geopolymer containing brick waste," *Cement and Concrete Composites*, vol. 138, p. 104943, 2023.

[37] J. L. Provis and J. S. Van Deventer, *Alkali activated materials: state-of-the-art report, RILEM TC 224-AAM*, vol. 13. Springer Science & Business Media, 2013.

[38] N. Ranjbar, C. Kuenzel, J. Spangenberg, and M. Mehrali, "Hardening evolution of geopolymers from setting to equilibrium: A review," *Cement and Concrete Composites*, vol. 114, p. 103729, 2020.

[39] S. C. Figueiredo, C. R. Rodríguez, Z. Y. Ahmed, D. H. Bos, Y. Xu, T. M. Salet, O. Çopuroğlu, E. Schlangen, and F. P. Bos, "An approach to develop printable strain hardening cementitious composites," *Materials & Design*, vol. 169, p. 107651, 2019.

[40] S. K. Das, S. K. Singh, J. Mishra, and S. M. Mustakim, "Effect of rice husk ash and silica fume as strength-enhancing materials on properties of modern concrete—a comprehensive review," *Emerging Trends in Civil Engineering: Select Proceedings of ICETCE 2018*, pp. 253–266, 2020.

[41] Ü. Yurt, "High performance cementless composites from alkali activated ggbfs," *Construction and Building Materials*, vol. 264, p. 120222, 2020.

[42] N. R. Rakhimova, "Recent advances in blended alkali-activated cements: A review," *European Journal of Environmental and Civil Engineering*, vol. 26, no. 10, pp. 4596–4618, 2022.

[43] J. L. Provis and S. A. Bernal, "Geopolymers and related alkali-activated materials," *Annual Review of Materials Research*, vol. 44, no. 1, pp. 299–327, 2014.

[44] C. Shi, D. Roy, and P. Krivenko, *Alkali-activated cements and concretes*. CRC press, 2003.

[45] Y. Alrefaei, Y.-S. Wang, J.-G. Dai, and Q.-F. Xu, "Effect of superplasticizers on properties of one-part ca (oh) 2/na2so4 activated geopolymer pastes," *Construction and Building Materials*, vol. 241, p. 117990, 2020.

[46] B. Mithun and M. C. Narasimhan, "Self-cured alkali activated slag concrete mixes-an experimental study," *International Journal of Civil and Environmental Engineering*, vol. 8, no. 4, pp. 477–482, 2014.

[47] M. R. Ahmad, B. Chen, and S. F. A. Shah, "Influence of different admixtures on the mechanical and durability properties of one-part alkali-activated mortars," *Construction and Building Materials*, vol. 265, p. 120320, 2020.

[48] A. Alujas, R. Fernández, R. Quintana, K. L. Scrivener, and F. Martirena, "Pozzolanic reactivity of low grade kaolinitic clays: Influence of calcination temperature and impact of calcination products on opc hydration," *Applied Clay Science*, vol. 108, pp. 94–101, 2015.

[49] J. Ren, B. C. Acarturk, N. D. Dowdy, and W. V. Srubar III, "The effects of calcium carbonate on sodium metasilicate-activated metakaolin-based geopolymer pastes," *Construction and Building Materials*, vol. 448, p. 138218, 2024.

[50] M. Samadi, L. S. Wong, G. Murali, N. H. A. S. Lim, I. Abdulkadir, S. Q. Tan, and Y. T. Chan, "Sodium metasilicate-activated one-part geopolymer concrete: Impact strength assessment with bottom ash substitution and fiber reinforcement," *Case Studies in Construction Materials*, vol. 21, p. e03794, 2024.

[51] Y. Zhang, H. Liu, T. Ma, G. Gu, C. Chen, and J. Hu, "Understanding the changes in engineering behaviors and microstructure of fa-gbfs based geopolymer paste with addition of silica fume," *Journal of Building Engineering*, vol. 70, p. 106450, 2023.

[52] G. Murali, A. K. Nassar, M. Swaminathan, P. Kathirvel, and L. S. Wong, "Effect of silica fume and glass powder for enhanced impact resistance in ggbfs-based ultra high-performance geopolymer fibrous concrete: An experimental and statistical analysis," *Defence Technology*, 2024.

[53] A. Alhamoud, H. T. Riahi, and A. Ataei, "Mechanical properties and stress-strain relationship of slag-based one-part geopolymer concrete: A comparative study," *Results in Engineering*, vol. 24, p. 102952, 2024.

[54] Z. Ou, R. Feng, F. Li, G. Liu, and N. Li, "Development of drying shrinkage model for alkali-activated slag concrete," *Construction and Building Materials*, vol. 323, p. 126556, 2022.

[55] J. Yu, F. Ji, Q. Lv, W. Li, Z. Lin, and Y. Peng, "Mechanical property and microstructure of fly ash-based geopolymer by calcium activators," *Case Studies in Construction Materials*, vol. 21, p. e03811, 2024.

[56] J. Qiao, Y. Lv, H. Peng, W. Han, B. Pan, and B. Zhang, "Performance and characterization of fly ash-metakaolin-based geopolymer pastes," *Materials Today Communications*, vol. 41, p. 110293, 2024.

[57] S. Xiaoshuang, S. Yanpeng, L. Jinqian, Z. Yuhao, and H. Ruihan, "Preparation and performance optimization of fly ash-slag-red mud based geopolymer mortar: Simplex-centroid experimental design method," *Construction and Building Materials*, vol. 450, p. 138573, 2024.

[58] M. A. Longhi, E. D. Rodriguez, B. Walkley, D. Eckhard, Z. Zhang, J. L. Provis, and A. P. Kirchheim, "Metakaolin-based geopolymers: Efflorescence and its effect on

microstructure and mechanical properties," *Ceramics International*, vol. 48, no. 2, pp. 2212–2229, 2022.

[59] S. Dadsetan, H. Siad, M. Lachemi, and M. Sahmaran, "Extensive evaluation on the effect of glass powder on the rheology, strength, and microstructure of metakaolin-based geopolymer binders," *Construction and Building Materials*, vol. 268, p. 121168, 2021.

[60] A. S. Srinivasa, K. Swaminathan, and S. C. Yaragal, "Effect of slag and solid activator on flowability and compressive strength of fly ash based one-part geopolymer pastes," *Materials Today: Proceedings*, 2023.

[61] M. Tuyan, Ö. Andiç-Çakir, and K. Ramyar, "Effect of alkali activator concentration and curing condition on strength and microstructure of waste clay brick powder-based geopolymer," *Composites Part B: Engineering*, vol. 135, pp. 242–252, 2018.

[62] M. Chaitanya, T. Nagaraju, L. Gadhiraju, V. Madepalli, and S. N. R. Jampana, "Strength and micro-structural performance of geopolymer concrete using highly burned rice husk ash," *Materials Today: Proceedings*, 2023.

[63] F. Hamidi, A. Valizadeh, and F. Aslani, "The effect of scoria, perlite and crumb rubber aggregates on the fresh and mechanical properties of geopolymer concrete," in *Structures*, vol. 38, pp. 895–909, Elsevier, 2022.

[64] C. K. Yip, G. C. Lukey, J. L. Provis, and J. S. Van Deventer, "Effect of calcium silicate sources on geopolymerisation," *Cement and Concrete Research*, vol. 38, no. 4, pp. 554–564, 2008.

[65] O. A. Mohamed, "Effects of the curing regime, acid exposure, alkaline activator dosage, and precursor content on the strength development of mortar with alkali-activated slag and fly ash binder: A critical review," *Polymers*, vol. 15, no. 5, p. 1248, 2023.

[66] T. Aydın, Z. B. Bundur, K. Aksoy, B. Karabıyık, E. Perin, T. İnce, and M. Sarı, "Utilization of stone wool kiln ash in cement-based materials," *Materials Proceedings*, vol. 15, no. 1, p. 89, 2024.

[67] P. He, M. Wang, S. Fu, D. Jia, S. Yan, J. Yuan, J. Xu, P. Wang, and Y. Zhou, "Effects of si/al ratio on the structure and properties of metakaolin based geopolymer," *Ceramics international*, vol. 42, no. 13, pp. 14416–14422, 2016.

[68] T. Wang, X. Fan, and C. Gao, "Strength, pore characteristics, and characterization of fly ash-slag-based geopolymer mortar modified with silica fume," in *Structures*, vol. 69, p. 107525, Elsevier, 2024.

[69] I. . P. 1), "Non-destructive testing of concrete-methods of test part 1 ultrasonic pulse velocity," 1992.

[70] J. J. Thomas, A. J. Allen, and H. M. Jennings, "Density and water content of nanoscale solid c–s–h formed in alkali-activated slag (aas) paste and implications for chemical shrinkage," *Cement and Concrete Research*, vol. 42, no. 2, pp. 377–383, 2012.

[71] M. Mastali, P. Kinnunen, A. Dalvand, R. M. Firouz, and M. Illikainen, "Drying shrinkage in alkali-activated binders–a critical review," *Construction and Building Materials*, vol. 190, pp. 533–550, 2018.

[72] B. Yuan, Q. Yu, E. Dainese, and H. Brouwers, "Autogenous and drying shrinkage of sodium carbonate activated slag altered by limestone powder incorporation," *Construction and Building Materials*, vol. 153, pp. 459–468, 2017.

[73] Y. Lou, M. Huang, S. Kang, M. Hu, W. Wu, and S. Chen, "Study on basic performance and drying shrinkage of binary solid waste geopolymer prepared with recycled powders and slag," *Case Studies in Construction Materials*, vol. 20, p. e03195, 2024.

[74] H. Taghvayi, K. Behfarnia, and M. Khalili, "The effect of alkali concentration and sodium silicate modulus on the properties of alkali-activated slag concrete," *Journal of Advanced Concrete Technology*, vol. 16, no. 7, pp. 293–305, 2018.

[75] X. Hu, C. Shi, Z. Zhang, and Z. Hu, "Autogenous and drying shrinkage of alkali-activated slag mortars," *Journal of the American Ceramic Society*, vol. 102, no. 8, pp. 4963–4975, 2019.

[76] A. Nadarajah, N. A. M. Nasir, N. A. Bakar, and N. A. Safiee, "Fly ash-ggbs blended geopolymer mortar for early engineering characteristic at ambient temperature," *Ain Shams Engineering Journal*, vol. 15, no. 7, p. 102821, 2024.

[77] B. Sun, P. Hao, J. Liu, Y. Wang, and Y. Li, "The driving mechanism of cement hydrated products leaching on as-built cement concrete bridge deck pavements," *Construction and Building Materials*, vol. 324, p. 126602, 2022.

[78] Z. Zhang, J. L. Provis, X. Ma, A. Reid, and H. Wang, "Efflorescence and subflorescence induced microstructural and mechanical evolution in fly ash-based geopolymers," *Cement and concrete composites*, vol. 92, pp. 165–177, 2018.

[79] L. Kuang, G. Li, J. Xiang, W. Ma, and X. Cui, "Effect of seawater on the properties and microstructure of metakaolin/slag-based geopolymers," *Construction and Building Materials*, vol. 397, p. 132418, 2023.

[80] C. Chen, S. Shenoy, K. Sasaki, H. Zhang, and Q. Tian, "Influence of liquid-to-solid ratios on properties and microstructure of coal gasification slag-based one-part geopolymer," *Case Studies in Construction Materials*, vol. 20, p. e02924, 2024.

[81] D. Zhang, T. Zhu, Q. Yang, V. Vandeginste, and J. Li, "Influence of ground granulated blast furnace slag on recycled concrete powder-based geopolymer cured at ambient temperature: Rheology, mechanical properties, reaction kinetics and air-void characteristics," *Construction and Building Materials*, vol. 438, p. 137190, 2024.

APPENDICES

APPENDIX A. SAMPLE PHOTOS FROM EACH EXPERIMENT

Figure A.1: *Flexural strength test apparatus with test sample*

Figure A.2: *Compressive strength test apparatus with test sample*

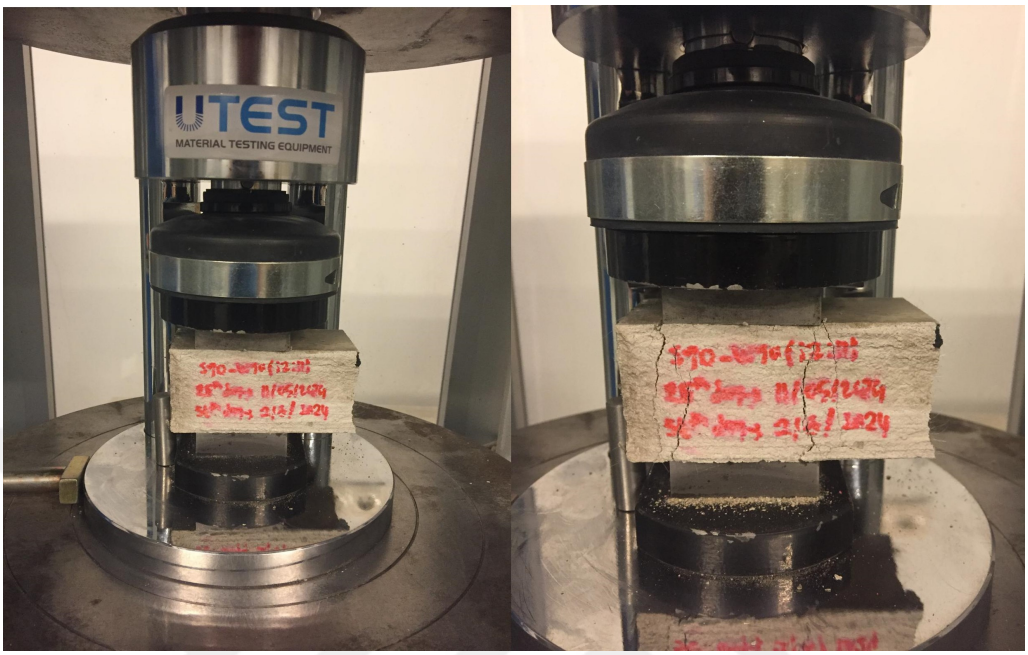

Figure A.3: *View of fiber distribution after flexural strength test*

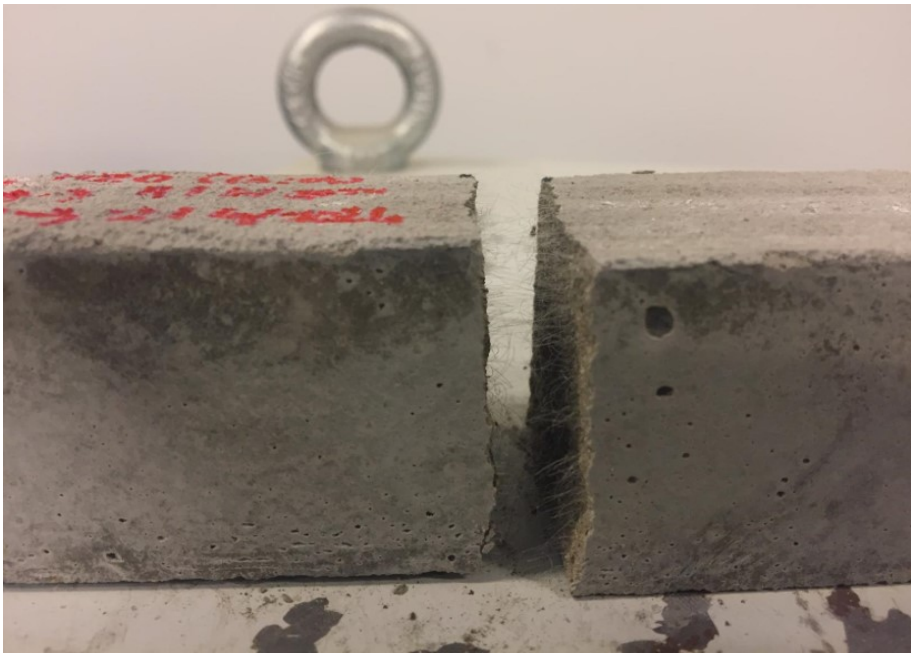

Figure A.4: *Application of UPV test in test sample*

Figure A.5: *Drying shrinkage setup*

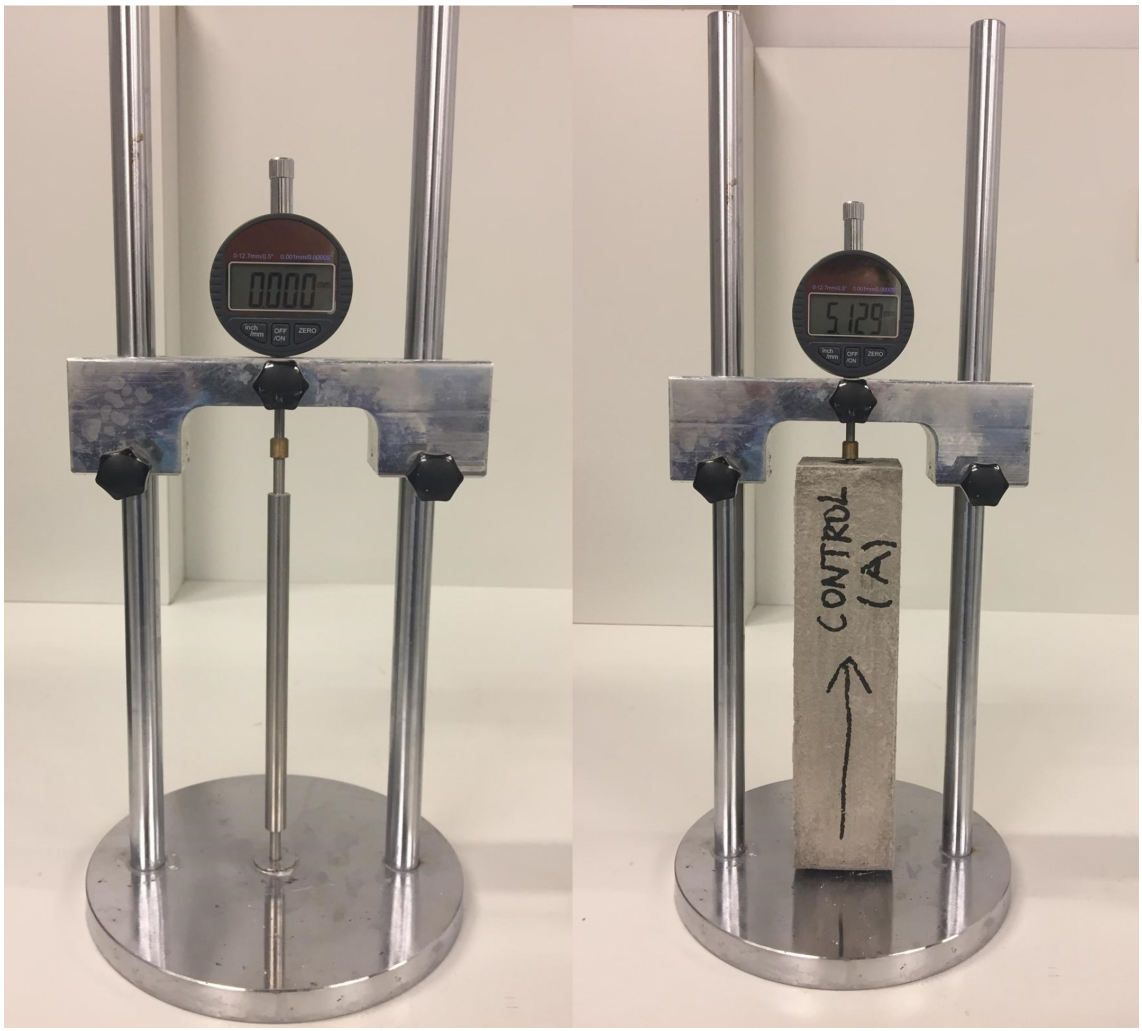

Figure A.6: *Alkali leaching observation*

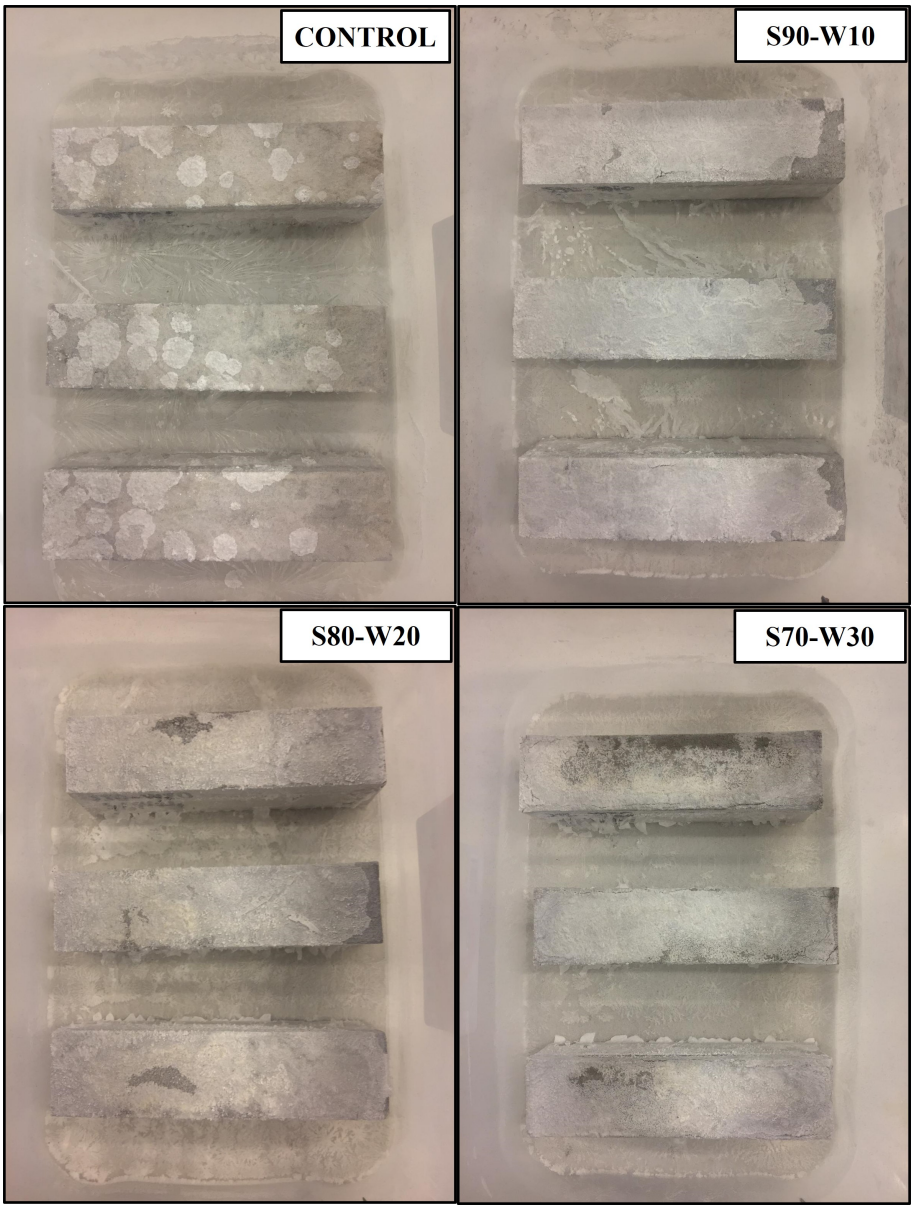

Figure A.7: *Core matrix structure of geopolymer paste at 28 days*